

# CHALMERS



## WIND TURBINE NOISE PROPAGATION OVER FLAT GROUND

MEASUREMENTS AND PREDICTIONS USING A PARABOLIC  
EQUATION METHOD

Master's Thesis in the Master's program in Sound and Vibration

IRÈNE LAURET DUCOSSON

Department of Civil and Environmental Engineering  
*Division of Applied Acoustics*  
*Vibroacoustics Group*  
CHALMERS UNIVERSITY OF TECHNOLOGY  
Göteborg, Sweden 2006

Master's Thesis 2006:10





MASTER'S THESIS 2006:10

# Wind turbine noise propagation over flat ground

Measurements and predictions using a Parabolic Equation method

Master's Thesis in the Master's program in Sound and Vibration

IRÈNE LAURET DUCOSSON

Department of Civil and Environmental Engineering  
*Division of Applied Acoustics*  
*Vibroacoustics Group*  
CHALMERS UNIVERSITY OF TECHNOLOGY  
Göteborg, Sweden 2006

Wind turbine noise propagation over flat ground  
Measurements and predictions using a Parabolic Equation method

© IRÈNE LAURET DUCOSSON, 2006

Master's Thesis 2006:10

Department of Civil and Environmental Engineering  
Division of Applied Acoustics  
Vibroacoustics Group  
Chalmers University of Technology  
SE-41296 Göteborg  
Sweden

Tel. +46-(0)31 772 1000

Cover:  
Wind turbine in Annelöv, Skåne, Sweden

Reproservice / Department of Civil and Environmental Engineering  
Göteborg, Sweden 2006

Wind turbine noise propagation over flat ground  
Measurements and predictions using a parabolic equation method  
Master's Thesis in the Master's program in Sound and Vibration  
IRÈNE LAURET DUCOSSON  
Department of Civil and Environmental Engineering  
Division of Applied Acoustics  
Vibroacoustics Group  
Chalmers University of Technology

## Abstract

Noise is one hindrance to the development of wind energy, and an extensive development of wind turbines calls for accurate predictions of the wind turbine noise. The standard for wind turbine noise prediction used in Sweden and many other countries does not take into account variations due to meteorological conditions. It can therefore be questioned whether it can satisfactorily predict wind turbine noise immission at long distances from the turbine.

In this thesis, an alternate model for outdoor sound propagation is designed using the Parabolic Equation (PE) method, for a flat land case. It includes atmospheric parameters and uses a logarithmic wind profile to model the influence of wind on the sound speed. The designed model is validated with comparisons to an existing model (Fast Field Program).

The aim of this study is to compare calculations based on the Swedish standard to measurements of noise immission. A further aim is to determine how well the PE method predicts the noise immission measurements. Finally the meteorological influence on immission levels is evaluated.

Simultaneous measurements of acoustic data and meteorological variables were performed over a month in order to provide a realistic set of atmospheric conditions and sound pressure levels. The measurements were examined in terms of total, A-weighted sound pressure levels, and their dependence on the wind speed at 10 m height and on the temperature gradient. The results showed a relation between the measured sound pressure levels and the wind speed, due to the increased source strength with increased wind speed. The influence on sound propagation of the meteorology was studied and found to be negligible for the setting and assumed profiles.

Significant deviations were shown between the results from the measurements and those from calculations, using different prediction methods: the method according to the standard, the PE method, the ray-based method WiTuProp, and an analytical solution. The prediction methods all underestimated the measured results, by about 5 to 8 dB in A-weighted sound pressure levels. The prediction methods tried in this study agree fairly well and the underestimation of the measured sound pressure levels is believed to be due to a possible error in the model of the source output sound power.

**Keywords:** wind turbine noise, outdoor sound propagation, refraction, Swedish standard for wind turbine noise, Parabolic Equation method.



# Contents

<b>Abstract</b>	<b>I</b>
<b>Preface</b>	<b>VII</b>
<b>Aknowledgements</b>	<b>VII</b>
<b>Notations</b>	<b>VIII</b>
<b>1 Introduction</b>	<b>1</b>
<b>2 Theory and background: outdoor sound propagation</b>	<b>5</b>
2.1 Atmospheric acoustics . . . . .	5
2.2 Sound propagation in homogeneous medium . . . . .	6
2.2.1 Spreading of the sound waves . . . . .	6
2.2.2 Atmospheric absorption . . . . .	7
2.2.3 Ground reflection . . . . .	8
2.3 Sound propagation in inhomogeneous medium . . . . .	10
2.3.1 Atmospheric refraction . . . . .	10
2.3.2 Turbulence effects . . . . .	12
2.4 Fundamental prediction methods . . . . .	14
2.4.1 Swedish standard for wind turbine noise . . . . .	14
2.4.2 Fast Field Program (FFP) . . . . .	14
2.4.3 Parabolic Equation method (PE) . . . . .	14
<b>3 Implementation of the sound propagation model</b>	<b>17</b>
3.1 Calculation model . . . . .	17
3.1.1 Fast Field Program . . . . .	17
3.1.2 Parabolic Equation method . . . . .	18
3.2 Impedance model . . . . .	20
3.2.1 Brief description of ground impedance . . . . .	20
<b>CHALMERS, Civil and Environmental Engineering, Master's Thesis 2006:10</b>	<b>III</b>

3.2.2	Influence of ground impedance . . . . .	21
3.3	Sound speed profile . . . . .	22
3.3.1	Linear profile . . . . .	22
3.3.2	Logarithmic profile . . . . .	23
3.4	Validation . . . . .	24
3.4.1	Comparison to analytical solution . . . . .	25
3.4.2	Comparison to a FFP calculation . . . . .	26
<b>4</b>	<b>Measurements</b>	<b>29</b>
4.1	Introduction . . . . .	29
4.2	Test set-up . . . . .	29
4.2.1	Measurement site . . . . .	29
4.2.2	Acoustic measurements and equipment . . . . .	31
4.2.3	Meteorological measurements and equipment . . . . .	31
4.3	Data processing . . . . .	32
4.3.1	Calibration . . . . .	33
4.3.2	Extraction of the frequency content . . . . .	33
4.3.3	Determination of sound pressure levels . . . . .	34
4.4	Conclusion . . . . .	34
<b>5</b>	<b>Analysis and results</b>	<b>35</b>
5.1	Analysis . . . . .	35
5.1.1	Estimation of the source output sound power . . . . .	35
5.1.2	Estimation of the background noise . . . . .	36
5.1.3	Selection of the data . . . . .	38
5.1.4	Statistical treatment of the data . . . . .	38
5.2	Results . . . . .	40
5.2.1	Measurements . . . . .	40
5.2.2	Swedish standard calculations . . . . .	42
5.2.3	PE calculations . . . . .	43
5.3	Discussion . . . . .	48
5.3.1	Methodological considerations . . . . .	48
5.3.2	Main findings . . . . .	49
<b>6</b>	<b>Conclusion</b>	<b>51</b>
<b>A</b>	<b>Fast Field Program FFP</b>	<b>53</b>

A.1	Solution of the Helmholtz equation . . . . .	53
A.2	Extrapolation from the ground and the top to the source . . . . .	55
A.3	Deformation of the integration path . . . . .	57
<b>B</b>	<b>Parabolic Equation (PE) method</b>	<b>59</b>
B.1	Crank-Nicholson PE . . . . .	59
B.2	Narrow-angle CNPE . . . . .	61
B.3	Wide-angle CNPE . . . . .	63
B.4	Finite-difference solution of the CNPE . . . . .	63
B.5	Boundary condition at the ground surface . . . . .	66
B.6	Upper boundary condition . . . . .	67
B.7	Starting field . . . . .	67
<b>C</b>	<b>Statistical analysis</b>	<b>69</b>
C.1	Regression line . . . . .	69
C.2	Residual variation . . . . .	70
C.3	Confidence intervals . . . . .	70
C.3.1	Slope . . . . .	70
C.3.2	Estimated $Y$ for a given $X$ . . . . .	71
C.3.3	Intercept . . . . .	71
	<b>References</b>	<b>74</b>



## Preface

This Master's Thesis gets onto the acoustical areas of outdoor sound propagation and numerical modeling. It was written from September 2005 to August 2006, at the department of Applied Acoustics, Chalmers University of Technology. The work is part of a research project on wind turbine noise, carried out at Miljömedicin, Göteborgs Universitet.

## Aknowledgements

I would like to thank the following people for their help and support along this work:

Jens Forssén, my supervisor at Chalmers,

Kerstin Persson Waye and Eja Pedersen, responsible for the project at Miljömedicin,

Martin Björkman for taking care of all the technical and practical aspects of this work,

the department of Applied Acoustics, and especially Börge Wijk for his help with the computers, Gunilla Skog for the administrative support and Maarten Hornikx.

Many other people contributed to this work by providing the data I needed:

Johan Hansson, Karin Wetterhill and Sylvia Broneske, Enercon GmbH

Pontus Thorsson, Akustikverkstan i Skaraborg AB

Anders Andersson, Vattenfall AB

Conny Larsson and Karin Törnblom, Uppsala University

Finally, I thank Kent Nilsson for his backyard in Annelöv

Göteborg, November 30, 2006

Irène Lauret Ducosson

## Notations

### *Abbreviations*

FFP	Fast Field Program
PE	Parabolic Equation
STFT	Short-time Fourier Transform

### *Roman upper case letters*

$A$	constant	
$D$	amplitude	
$L$	level	(dB)
$Q$	reflection coefficient	(-)
$Q$	Fourier transformed variable $q_c$	
$R$	propagation distance	(m)
$R_{max}$	maximum range of calculation domain	(m)
$T$	temperature	(K)
$Z$	normalized ground impedance	
$Z_{max}$	maximum height of calculation domain	(m)

### *Roman lower case letters*

$a$	linear refraction parameter	( $m^{-1}$ )
$b$	logarithmic refraction parameter	(m/s)
$c$	sound speed	(m/s)
$f$	frequency	(Hz)
$k$	wave number	(rad/m)
$p$	acoustic pressure	(Pa)
$q$	square root operator variable	
$r$	position (m)	
$t$	time	(s)
$v$	wind component	(m/s)
$z$	height	(m)
$z_0$	roughness length	(m)

### *Greek upper case letters*

$\Delta$	variation
----------	-----------

### *Greek lower case letters*

$\alpha$	angle from wind direction to propagation direction	( <i>rad</i> )
$\alpha_e$	Attenborough parameter	( $m^{-1}$ )
$\beta$	elevation angle	( <i>rad</i> )
$\gamma$	ratio of air specific heats	( $-$ )
$\delta$	delta function	
$\epsilon$	average height of ground irregularities	( <i>m</i> )
$\zeta$	acoustic impedance	
$\theta$	angle of incidence	( <i>rad</i> )
$\sigma$	flow resistivity	( <i>Pa.s/m<sup>2</sup></i> )
$\sigma_e$	Attenborough parameter	( <i>Pa.s/m<sup>2</sup></i> )
$\psi$	envelope solution for the 2D Helmholtz equation	
$\omega$	angular frequency	( <i>rad/s</i> )

### *Subscripts*

0	reference
1	direct
2	reflected
<i>air</i>	air
<i>c</i>	complex
<i>eff</i>	efficient
<i>n</i>	normal
<i>p</i>	pressure
<i>r</i>	receiver
<i>ref</i>	reference
<i>r, <math>\theta, z</math></i>	cylindrical coordinates
<i>s</i>	source
<i>t</i>	truncation

### *Notations*

$\hat{\cdot}$	amplitude
$\vec{\cdot}$	vector
$\ \cdot\ $	norm
$ \cdot $	absolute value



# Chapter 1

## Introduction

---

The problem of noise pollution induced by the operation of wind turbines is an important public health issue. The regulations relative to wind turbine noise impose lower and lower admissible sound pressure levels. Hence, there is a deep interest in predicting accurately the immission levels. The introduction presents the work carried out in this thesis.

---

### Thesis background

The installation of wind turbines is increasing in Sweden. It can induce a higher proximity to living areas and involve a growing sensibility to wind turbine noise. Although there is a demand for renewable energy, wind turbine noise is one major hindrance to the wide development of wind energy.

In the planning process of wind turbine installation, the noise immission levels at the nearest houses are assessed with a calculation made according to the Swedish standard for wind turbine noise (Swedish Environmental Protection Agency 2001). This standard does not include variations of meteorological data in its outdoor sound propagation model. It can therefore be questioned whether it satisfactory predicts wind turbine noise immission at long distances from the turbine.

As already described in literature (Larsson 2000), the propagation of sound is influenced by the state of the atmosphere, through refraction, absorption and scattering by turbulence. Vertical wind speed profiles and temperature gradients cause refraction, i.e. curving of the sound rays. In downwind conditions or for positive temperature gradients the sound rays are bent toward the ground, which can cause strong focusing effects of the propagated sound. In upwind conditions or for negative temperature gradients the sound rays are bent upward, creating so-called sound shadow zones, areas which no sound rays can reach.

Absorption occurs when sound propagates through air and modifies the frequency content of the sound. It depends on frequency, relative humidity, temperature and atmospheric pressure.

Turbulence causes random fluctuations of wind velocity and temperature, thus fluctuations of sound speed. Turbulence has a double effect on sound propagation. First, it has a scattering effect which can spread out the sound, also into silent

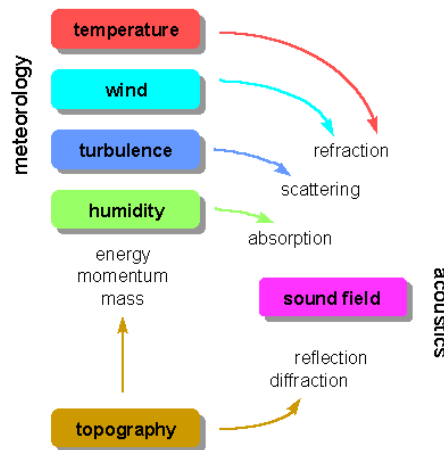


Figure 1.1: *Sound propagation in the atmosphere.*

zones. Secondly, it causes fluctuations of the phase and amplitude of the sound wave, thus destroying the interference between the sound rays reaching the receiver. This can give higher sound pressure levels than theoretically expected.

Today, a good model for noise propagation, including the influence of meteorological parameters, is needed in order to describe and predict accurately wind turbine noise levels.

## Thesis aim

An outdoor sound propagation model is to be implemented, including meteorological parameters. The designed model aims at predicting accurately wind turbine noise propagation. Several numerical methods for atmospheric acoustics have previously been developed, which include the meteorological parameters, among which the Parabolic Equation method is well established.

In the following, measurements carried out on a flat land area are touched upon. The Master's thesis is made in cooperation with Miljömedicin, Göteborgs Universitet. Thanks to their equipment, sound and meteorological data is recorded, and additional data can be retrieved from the plant operator. The outdoor sound propagation model is calculated with the Parabolic Equation (PE) method, and a testing model is based on the Fast Field Program (FFP).

The study aims at three points: first, to compare the Swedish standard calculations to the measurements results; second, to determine if the PE method can give better prediction of wind turbine noise propagation; finally, to determine how large the meteorological influence is on immission levels at receiver point and what the reasons are for possible deviations between measurements and calculations.

## Previous work

The starting point of this project is an article by van den Berg (2003). A description of wind turbine noise perception is given: "residents living 500 m and more from the wind turbines have reacted strongly to the noise; residents up to 1900 m distance expressed annoyance. A resident living at 1.5 km from the wind turbines describes the sound as an endless train". Annoyance is expressed in spite of existing Dutch sound assessment and regulations.

According to van den Berg (2003), including meteorological condition variations gives a better prediction of sound propagation. Larsson (2000) also gets onto the weather effects on outdoor sound propagation and the importance of including weather data in sound propagation predictions.

Different international and national standards exist aiming at assessing wind turbine noise. However, they fail at accurately predict the noise levels. As a consequence, debates have arisen worldwide (e.g. United States, United Kingdom, Germany). An international conference in October 2005 in Berlin, "Perspectives for control of wind turbine noise", presented topics such as

- the modeling of wind farms noise (Sloth 2005),
- the localization of noise sources on a wind turbine (Oerlemans and López 2005),
- the validity of wind speed measurements for assessment of wind turbine noise (Botha 2005),

However, very few corrected models for sound propagation were presented. In Australia, the regulations for wind turbine noise are based on a ray theory heuristic model; but this model seems to disagree with other methods, and needs further validation studies (Tickell 2005). Another model, also based on ray theory, is developed by Delta Acoustics & Vibration in Denmark (Kragh and Sondergaard 2005).

For this thesis, the sound propagation is calculated with the numerical methods PE method and FFP. Salomons (2001) details thoroughly the mathematical scheme of these computational methods.

In Forssén (2001), a PE model for "Calculation of sound reduction by a screen in a turbulent atmosphere" is implemented. Hornikx (2003) developed PE codes for application to urban areas (canyon configuration) and flat land areas (reflecting ground configuration). The codes developed in these works are available at the Division of Applied Acoustics. They comprise of the support for the numerical propagation model implemented in this thesis.

## Thesis overview

- Chapter 1 introduces the reader to the problem by giving the thesis background and aim. The presentation of previous works sets the starting point for the thesis and the main questions are touched upon.
- Chapter 2 aims at describing the particular field of atmospheric acoustics: notably, the main phenomena which influence the outdoor propagation of sound. Geometrical effects and atmosphere influence are presented, as well as different numerical methods.
- Chapter 3 details the implementation of the outdoor sound propagation model, based on the numerical methods FFP and PE. It also gives an overview of the models used to describe the physical properties of the measurement environment (ground impedance and sound speed profiles). Finally, a validation of the implemented model is made for several configurations.
- Chapter 4 describes measurements conducted during the measurement campaign in November-December 2005. The measurement set-up, the data acquisition and the post-processing are detailed.
- Chapter 5 presents the results of this study. The measured sound pressure levels are related to the sound propagation conditions with special emphasis on meteorological conditions. Furthermore, the measured sound pressure levels are compared to the Swedish standard predictions and to PE predictions in focus.
- Chapter 6 sums up the problem, the methods used and the results. It draws the conclusions made on basis of the results.

## Chapter 2

# Theory and background: outdoor sound propagation

---

The outdoor sound propagation is a complex process. It depends on a large number of parameters, related to the properties of the propagation medium (atmosphere), to the boundary conditions (ground surface) and to the position of source and receiver. This chapter presents the main phenomena influencing the propagated acoustic wave. The chapter gets onto the phenomena in an homogeneous medium and the effects related to inhomogeneous atmospheric parameters. Finally, the last section presents two numerical prediction methods: the Fast Field Program (FFP) and the Parabolic Equation (PE) method.

---

### 2.1 Atmospheric acoustics

The basic problem of outdoor sound propagation is described in Figure 2.1. A point source, located over the ground at height  $z_s$ , produces an acoustic wave that propagates through the atmosphere along a distance  $R$ , to a receiver, placed at a height  $z_r$ .

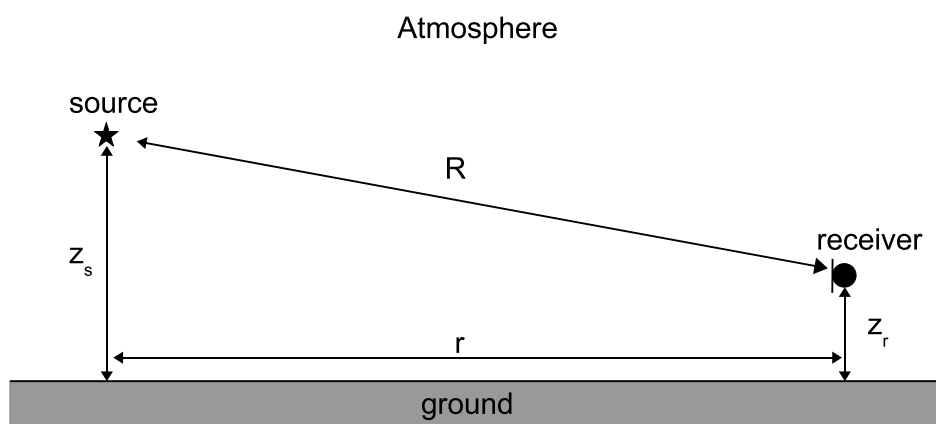


Figure 2.1: Basic geometry of outdoor sound propagation. Source and receiver are at heights  $z_s$  and  $z_r$  respectively. The acoustic wave propagates along the distance  $R$ .

Hence, the induced acoustic field depends on the values  $z_s$ ,  $z_r$ , and  $R$ , as well as the characteristics of the ground, the properties of the atmosphere and any possible sound speed profile. These diverse input parameters make the propagation of

sound in the atmosphere a complex process.

As a starting point, the sound propagation is assumed to be governed by the wave equation,

$$\nabla^2 p(\vec{r}) - \frac{1}{c^2(\vec{r})} \frac{\partial^2 p(\vec{r})}{\partial t^2} = -4\pi\delta(\vec{r} - \vec{r}_s) \quad (2.1)$$

where  $p$  is the acoustic pressure,  $\vec{r}$  is the space vector position and  $\vec{r}_s$  the source position,  $\delta$  is a delta function of unit strength,  $c(\vec{r})$  is the sound speed. The wave equation can be written for complex harmonic waves in the frequency domain using a Fourier transform. Omitting the time factor  $e^{-i\omega t}$ , where  $\omega$  is the angular frequency, it becomes the Helmholtz wave equation,

$$(\nabla^2 + k^2)p_c(\vec{r}) = -4\pi\delta(\vec{r} - \vec{r}_s) \quad (2.2)$$

where  $k = \frac{\omega}{c(\vec{r})}$  is the spatially varying wave number. All the outdoor sound propagation methods try to solve directly this equation.

## 2.2 Sound propagation in homogeneous medium

An homogeneous medium is characterized by its constant atmospheric parameters. As a result, the sound speed is constant. In an homogeneous medium, the sound propagation is influenced by three main phenomena:

- the spreading of sound waves, depending on the propagation length,
- the atmospheric absorption, depending on the propagation length, the medium characteristics and the frequency,
- the reflection on surfaces, leading to a loss of acoustic energy and a phase shift, depending on the surface properties.

### 2.2.1 Spreading of the sound waves

When a sound source radiates, the propagated sound waves spread in the surrounding space. This induces an acoustic attenuation independent of frequency and which is a function of the propagation length.

The complex sound pressure field of a harmonic spherical wave in free field is given as

$$p_{c,free} = A \frac{e^{ikR}}{R} \quad (2.3)$$

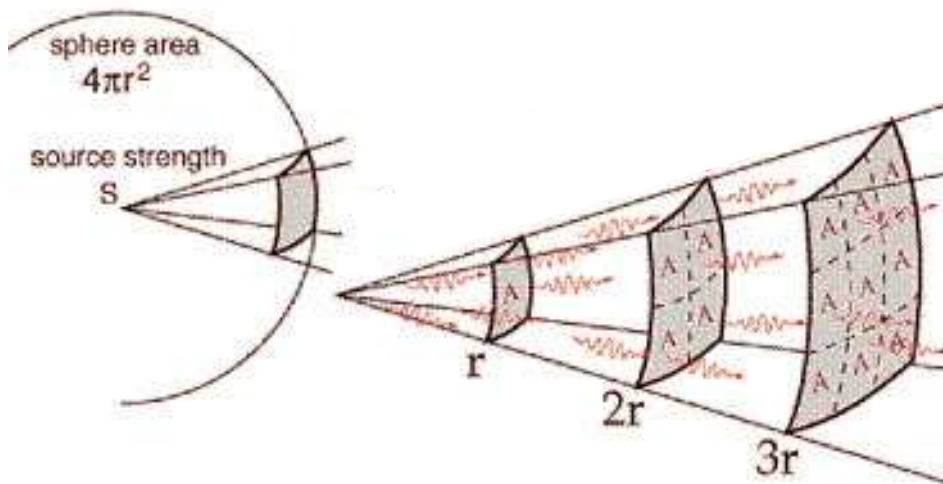


Figure 2.2: Radiation of point source in air.

where  $A$  is an amplitude, and  $R$  is the propagation length of the sound wave. Thus, the complex pressure amplitude is  $\hat{p}_c = \frac{A}{R}$ .

As a consequence,

- the squared pressure amplitude is proportional to  $\frac{1}{R^2}$ , and is divided by 4 for a doubling of propagation length,
- the sound pressure level,  $L_p = 10 \log \left( \frac{\tilde{p}^2}{\tilde{p}_0^2} \right)$ ,  $\tilde{p}_0 = 20 \mu\text{Pa}$ , decreases with 6 dB for a doubling of propagation length.

## 2.2.2 Atmospheric absorption

Sound waves traveling through the atmosphere also lose energy by dissipative processes. This phenomenon is known as the atmospheric absorption.

Atmospheric absorption involves the effects of fluid viscosity, energy transfer between the air molecules and thermal diffusion. The wave propagating in the atmosphere will cause the molecules to vibrate and rotate, leading to a transfer of energy from the sound wave to the air. Generally, atmospheric absorption should be taken into account for sound propagation over distances larger than 100 m.

In first approximation, the atmospheric absorption is proportional to the propagation distance and to an absorption coefficient that depends on the frequency and on the atmosphere temperature, pressure and air humidity. The calculation of the air absorption coefficient is made according to ISO 9613-1: 1993.

In Figure 2.3, the absorption coefficient is plotted as a function of frequency for different values of temperature, relative humidity and atmospheric pressure.

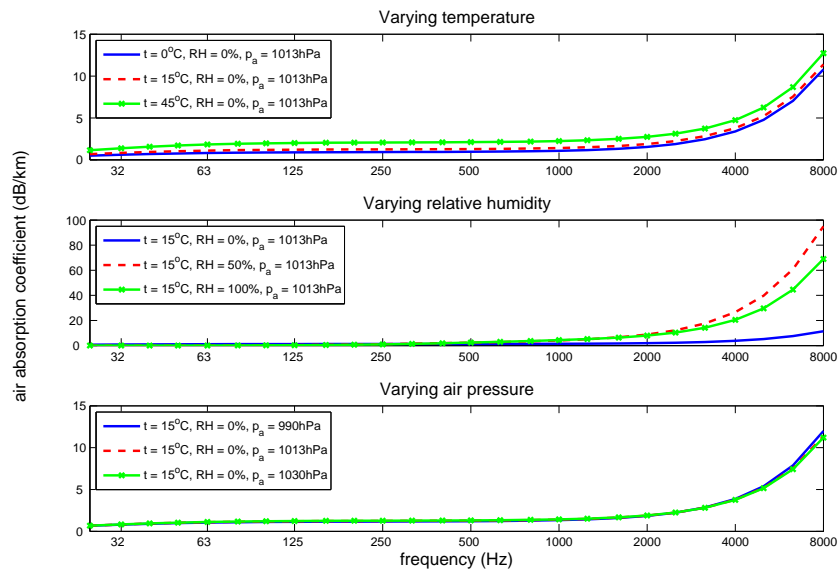


Figure 2.3: Absorption coefficient as a function of frequency for different values of relative humidity.

Figure 2.3 shows that the atmospheric absorption increases rapidly with the sound frequency, with the result that low frequencies are of more importance for long-range noise propagation. Different values for the temperature, relative humidity and atmospheric pressure were used to draw the graphs. They show that temperature and relative humidity are the parameters which most influence the absorption coefficient. The temperature has a noticeable effect over the whole range of frequency whereas the relative humidity influences the absorption coefficient very strongly only for high frequency (>1000 Hz).

Atmospheric absorption causes a decrease of the amplitude of the sound wave. It also has an effect on the speed of the sound wave. This effect varies with frequency leading waves with different frequencies to travel with different speeds (dispersion phenomenon). For most practical applications, however, this effect can be neglected.

### 2.2.3 Ground reflection

For real cases, both sound source and receiver positions are above a ground surface. This surface reflects sound waves, so the sound field at the receiver point results of the contribution of a direct wave and a reflected wave (see Figure 2.4).

The complex pressure field at the receiver in the geometry shown in Figure 2.4 is then

$$p_c = A \frac{e^{ikR_1}}{R_1} + Q.A \frac{e^{ikR_2}}{R_2} \quad (2.4)$$

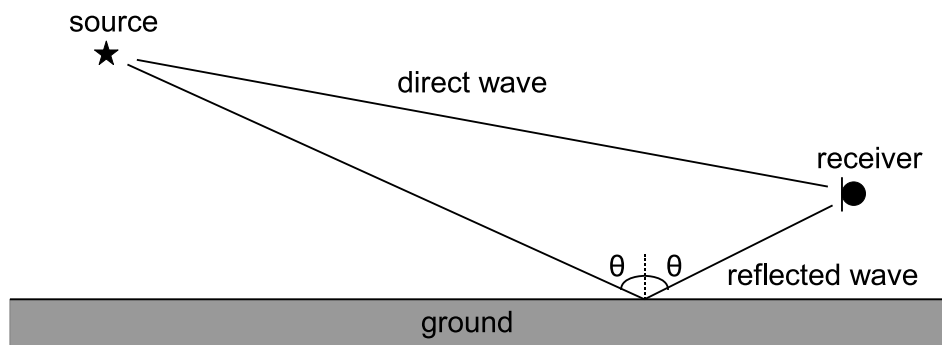


Figure 2.4: Source and receiver above a ground surface. Reflection of the sound wave.

where  $R_1$  and  $R_2$  are, respectively, the direct and reflected sound wave paths, expressed as

$$\begin{aligned} R_1 &= \sqrt{r^2 + (z_s - z_r)^2} \\ R_2 &= \sqrt{r^2 + (z_s + z_r)^2} \end{aligned} \quad (2.5)$$

using the notations of Figure 2.1. The factor  $Q$  in Equation (2.4) is called the reflection coefficient and depends on the angle of incidence  $\theta$  and on the normalized ground impedance  $Z$ .

The normalized ground impedance  $Z$  characterizes the ground surface acoustically. It is a complex value, and depends on the sound wave frequency and on the ground surface structure.

The effective flow resistivity  $\sigma$  describes this ground structure. Typical  $\sigma$  values for natural absorbing grounds, such as grassland, forest floors or sandy grounds, range from  $\sigma = 10$  to  $1000 \text{ kPa}\cdot\text{s}/\text{m}^2$ .

Several models have been developed in order to calculate the normalized ground impedance (see Section 3.2). The most common one is the empirical model by Delany and Bazley (1970). Theoretical models also have been developed, such as the Attenborough model (Attenborough 1992).

For an acoustically hard ground, both  $Z = \infty$  and  $\sigma = \infty$ . The reflection coefficient is then close to 1. All the acoustic energy is reflected by the surface. An acoustically hard surface is usually referred to as a rigid surface. On the other hand, if the ground impedance is finite, the absolute value of the reflection factor is usually less than 1 and some of the acoustic energy is absorbed by the reflecting ground.

For practical situations, with not too low source and receiver positions, the reflection factor can be approximated as for the case of plane waves:

$$Q = \frac{Z \cos \theta - 1}{Z \cos \theta + 1} \quad (2.6)$$

Finally, the roughness of the ground surface also influences the reflection phenomenon. As a matter of fact, a random roughness can cause diffusion of the reflected wave. Moreover, the roughness can make the ground behave acoustically softer.

## 2.3 Sound propagation in inhomogeneous medium

In reality, the atmosphere is an inhomogeneous medium. The meteorological properties vary mainly depending on height and time. Therefore, the sound propagation through the atmosphere is affected by these varying parameters, and their effects should generally be considered for propagation path longer than 50 m.

### 2.3.1 Atmospheric refraction

Sound waves can be seen as rays traveling through the air. A spatial variation of the sound speed in the atmosphere causes the path that sound rays follow to change. Sound rays are bent toward regions where the sound speed is lower. This effect is known as atmospheric refraction.

The speed of sound in the atmosphere is a function of several factors. Assuming that the air is an ideal gas, the sound speed is mainly depending on the temperature and on the wind speed and direction.

#### Temperature effects

Vertical gradients of the temperature influence the sound speed in the atmosphere. The sound speed change as a function of the temperature  $T$  can be written as

$$c = c_0 \sqrt{\frac{T}{T_0}} \quad (2.7)$$

where  $T$  is the temperature in Kelvin.  $c_0$  is the sound speed at the temperature  $T_0$ : commonly,  $T_0 = 273K$  and  $c_0 = 343$  m/s.

For negative gradients of temperature, the sound rays are bent away from the ground. This phenomenon is called upward refraction (see Figure 2.5). Upward refraction causes a reduction of the sound pressure level near the ground, and the apparition of so-called shadow zones, with low sound levels.

On the contrary, positive gradients of temperature will cause the sound rays to bend toward the ground surface. This phenomenon is called downward refraction.

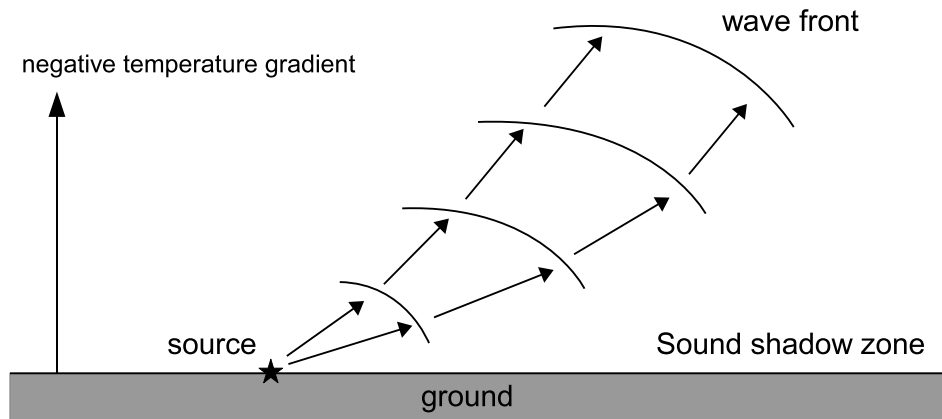


Figure 2.5: Upward refraction caused by negative temperature gradient. Apparition of a silent zone close to the ground.

For downward refraction case, the sound rays are concentrated near the ground. If the propagation path is long enough, the rays may be reflected more than once, making the ground surface properties very important. Downward refraction will therefore enhance long-range sound propagation.

### Wind effects

The presence of wind fields makes the atmosphere anisotropic, hence also influences the sound speed.

The wind in the atmosphere is represented by a vector of three components:

- an horizontal vector with two components,  $(v_r, v_\theta)$ ,
- a vertical vector with one component,  $v_z$ ,

where  $r$ ,  $\theta$  and  $z$  stand for the three space coordinates of the cylindric coordinate system.

The common solving methods for the wave equation are 2D-models. Therefore, only the  $r$ - and  $z$ -components of the wind field are considered. Moreover, the amplitude of  $v_z$  is approximately 10 times smaller than the amplitude of  $v_r$ , and  $v_z$  becomes negligible compared to  $v_r$  (Aballéa 2004). As a consequence, the effect of wind on the sound speed can be expressed as

$$c_{eff} = c_0 + \|\vec{v}\| \approx c_0 + v_r \quad (2.8)$$

where  $c_0$  is the sound speed without wind.  $c_{eff}$  is referred to as the effective sound speed. The strength of the refraction can thus be described by the acoustic refractive index,  $n = \frac{c_0}{c_{eff}}$ .

The introduction of the variable  $c_{eff}$  allows replacing a moving atmosphere by a non-moving atmosphere with an effective sound speed. This is an approximate approach, which is valid for small elevation angles, defined as

$$|z_r - z_s| \ll r \quad (2.9)$$

using the notations of Figure 2.1.

For a wind blowing in the direction opposite to the sound propagation, the wind velocity comes as a negative contribution to the sound speed and the sound rays are bent away from the ground. It results in upward refraction.

For a wind blowing in the same direction as the sound propagation, the opposite phenomenon occurs. The sound rays are bent toward the ground causing downward refraction.

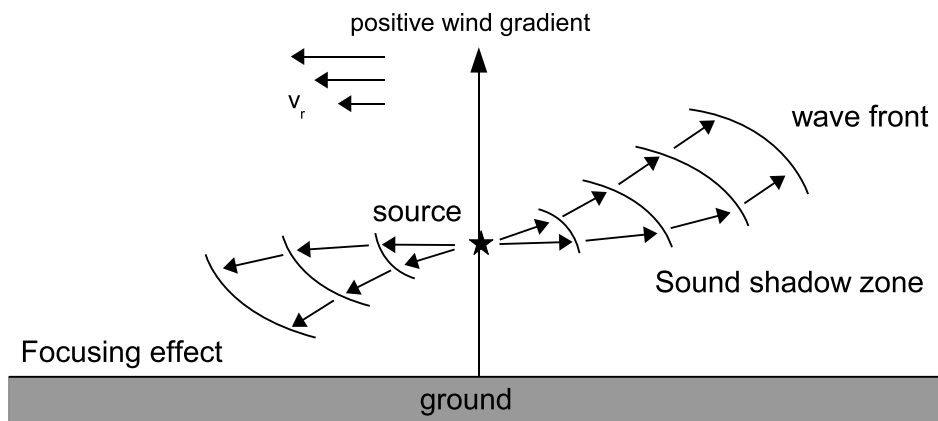


Figure 2.6: Refraction caused by wind gradient. Downward refraction in the wind direction, upward refraction against the wind direction.

For the general case where the sound propagation is not in the same direction as the wind, an approximate formula can be used

$$c_{eff} = c_0 + v_r \cdot \cos \alpha \quad (2.10)$$

where  $\alpha$  is the angle between the sound propagation direction and the wind direction. This means that  $c_{eff}$  is estimated as the sum of the sound speed without wind  $c_0$  and the projection of the wind speed  $v_r$  on the propagation direction.

### 2.3.2 Turbulence effects

The atmosphere is characterized as a turbulent medium. This implies that, on time scales of seconds or minutes, the temperature, wind and effective sound speed

profiles show fluctuations around average values. These instantaneous profiles have an important effect on atmospheric sound propagation, as, while the sound propagates through turbulence, scattering of the acoustic energy occurs.

In the case of a refracting atmosphere, the sound field is scattered by the turbulence eddies and becomes more diffuse than in the case of a non-turbulent refracting atmosphere. In a downward refracting turbulent atmosphere, the main effect of turbulence is a reduction of the interference between the direct and reflected sound waves.

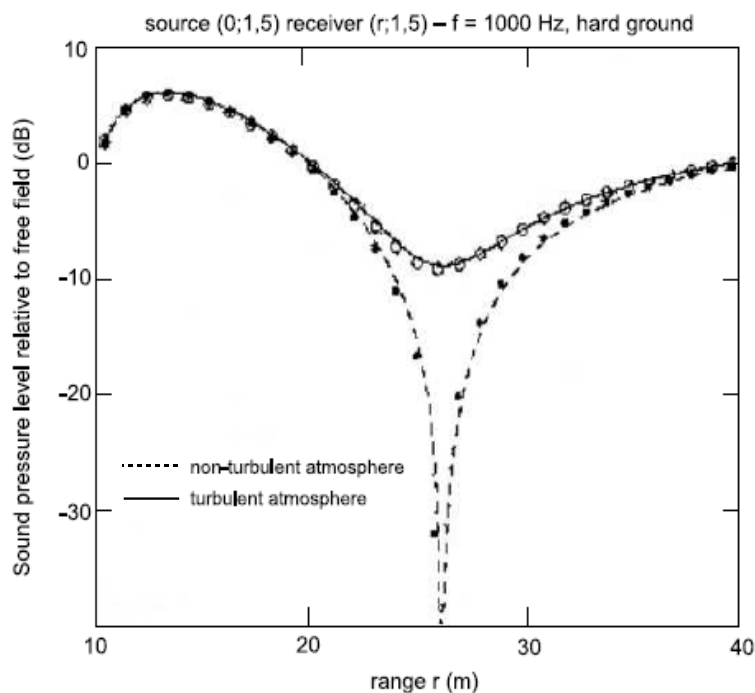


Figure 2.7: Sound pressure level plotted over range, with and without turbulence, in a downward refracting atmosphere. Source and receiver heights are set to 1,5 m. Calculation is made at 1 kHz.

In Figure 2.7, the dashed curve shows the typical dip of the interference pattern between the direct and ground reflected sound wave. For the geometry presented in this example, and without turbulence, the two waves cancel out around 26 m away from the source. In presence of turbulence, the sound is diffused and this negative interference disappears.

In an upward refracting turbulent atmosphere, the main effect of turbulence is the scattering of the sound waves into the shadow zones. This can be explained as small-scale refractions due to turbulence eddies.

## 2.4 Fundamental prediction methods

### 2.4.1 Swedish standard for wind turbine noise

The Swedish standard for wind turbine noise determines a assumed maximum value for the total, A-weighted sound pressure level (Swedish Environmental Protection Agency 2001). It corresponds to a case with a wind speed of 8 m/s at 10 m height. The standard distinguishes between propagation over land or water, and propagation over distances longer or shorter than 1000 m.

In the case of this study, sound propagation is over land, with distance shorter than 1000 m. For such case, the standard noise assessment in dBA is

$$L_P(A)_{tot} = L_W(A)_{tot} - 8 - 20 \cdot \log(r) - 0.005 \cdot r \quad (2.11)$$

where  $L_W(A)_{tot}$  is the total, A-weighted source output power, and  $r$  is the distance from the wind turbine to the receiver point. The factor 0.005 is a damping term which takes into account the global air and ground absorption.

### 2.4.2 Fast Field Program (FFP)

The Fast Field Program is a powerful and fast numerical method used for outdoor sound propagation. It gives an exact solution for the sound field in an homogeneous atmosphere, and allows an accurate description of the vertical meteorological profiles.

However, the FFP has some important limitations. The first one is directly linked to its principle which sets the ground impedance and the atmospheric parameters to be range independent.

The FFP was first developed for underwater acoustics before being adapted to outdoor sound propagation.

### 2.4.3 Parabolic Equation method (PE)

The PE method is a family of methods for calculating sound propagation in inhomogeneous medium. The PE method calculates the sound field stepwise along the propagation path, from the source to the receiver, from an initial monopole field. This allows for including range dependence of both ground and atmospheric conditions.

However, the solution is valid for the far-field only. Moreover, the parabolic equation solved in the method follows from the wave equation by neglecting contributions to the field from sound waves with large elevation angle. Consequently, the

PE method gives accurate results for a limited range of elevation angle, depending on this approximation.

The advantage of using the PE method instead of the new engineering methods (e.g. Nord2000 (Kragh and Sondergaard 2005), Harmonoise) is that an arbitrary sound speed profile can be included. In the new engineering methods, a linear profile is assumed. The disadvantage of the PE method is the calculation time.



# Chapter 3

## Implementation of the sound propagation model

---

This chapter aims at presenting the designed sound propagation model, for which the phenomena described in the previous chapter are taken into account. The first section concisely describes the FFP and PE method. More thorough descriptions can be found in the appendices. The second and third sections consist of the description of the ground models and sound speed profiles, candidates to the implemented model. Finally, a validation of the sound propagation model is made in the last section, for different configurations of the problem.

---

### 3.1 Calculation model

#### 3.1.1 Fast Field Program

The Fast Field Program is a numerical method for calculating the sound field produced by a monopole source above a ground surface, in a layered atmosphere. The ground is characterized by its impedance and the atmosphere is represented by the vertical profiles of the wind and the temperature.

The atmosphere is divided into a number of homogeneous layers. Within the layers, the profiles are approximated with a constant value for temperature and wind speed. This leads to a layered profile of both the sound speed and the wave number.

The solution is computed in each layer in the wave number domain, taking into account the appropriate continuity relations at the interface between the layers. The sound field is calculated in the space domain from the solution by an inverse Fourier transform.

The equation implemented for each layer is the homogeneous Helmholtz equation in the wave number domain:

$$\partial_z^2 Q + k_z^2 Q = -\sqrt{2\pi k_r} \delta(z - z_s) \quad (3.1)$$

with the notation  $\partial_r \equiv \frac{\partial}{\partial r}$  and  $\partial_z \equiv \frac{\partial}{\partial z}$ .  $Q$  is the Fourier transformed variable  $q_c = p_c \sqrt{r}$ , where  $p_c$  is the complex pressure amplitude and  $k_z$  is the wave number

along the  $z$ -axis,  $k_z^2 = k^2 + k_r^2$ . The source height is  $z_s$ .

After defining the boundary conditions, Equation (3.1) can be solved stepwise from the ground surface to the source height and from the top to the source height.

As stated in Section 2.4.2, the major drawback of the FFP, in its original formulation, is that it cannot handle range-dependent atmospheric parameters or ground impedance. Nor can it handle turbulence. Alternative versions of the FFP, which can include both range-dependent parameters and turbulence, are cited in Johansson (2003).

### 3.1.2 Parabolic Equation method

The Parabolic Equation (PE) method is a numerical method for computing the sound field of a monopole source in a refracting atmosphere above a ground surface. For outdoor propagation, the PE method allows a precise description of the atmosphere as both the sound speed profile and the ground impedance can vary along the propagation path. Moreover, atmospheric turbulence can be taken into account.

In the PE method, a marching algorithm calculates the sound field step by step, from an initial source field to the receiver. The Helmholtz wave equation is approximated by neglecting contributions to the field from sound waves with large elevation angles, leading to a parabolic equation. As a consequence, the PE method gives accurate results in a spacial region limited by a maximum elevation angle. Typically, the maximum elevation angle ranges from 10 to 70°.

Different PE methods for atmospheric acoustics have been developed since 1989. A method called the Crank-Nicholson PE (CNPE) is implemented. A flat, locally reacting ground surface is assumed in the CNPE method. Small scale roughness can be incorporated directly into the model by modifying the surface impedance. The effect of turbulence will not be included in this description.

#### Crank-Nicholson PE

In the Crank-Nicholson PE method, the axisymmetric approximation is assumed (i.e. rotational symmetry around the  $z$ -axis). Thus, only a plane in the  $r, z$ -domain is studied, and the propagation becomes two-dimensional. Several formulations exist for the Crank-Nicholson PE. The narrow-angle formulation is limited to very small propagation angles, the wide-angle formulation is less restrictive.

Assuming the axisymmetric approximation and the far-field approximation, the Helmholtz wave equation is reduced to the two-dimensional differential equation

$$\partial_r^2 q_c + \partial_z^2 q_c + k^2 q_c = 0 \quad (3.2)$$

where  $k$  is the wave number and  $q_c = p_c\sqrt{r}$ . The same notations as in Section 3.1.1 are used for the derivatives.

A solution to this equation can be written as

$$q_c = \psi(r, z) e^{ik_0 r} \quad (3.3)$$

where  $k_0$  is a reference wave number, at the ground for example. Introducing the operator  $\sqrt{1+q} = \sqrt{\frac{k^2}{k_0^2} + \frac{1}{k_0^2} \partial_z^2}$  and considering only the outgoing wave, Equation (3.2) becomes

$$\partial_r \psi = ik_0 \left( \sqrt{1+q} - 1 \right) \psi \quad (3.4)$$

Depending on the development of the root operator, different CNPE are formulated. The narrow-angle formulation is based on a linear expansion of the operator, and Equation (3.5) is implemented for the numerical model.

$$\partial_r \psi = ik_0 \frac{q}{2} \psi \quad (3.5)$$

The wide-angle formulation develops the operator as a quadratic function, and Equation (3.6) is implemented for the numerical model.

$$\left( 1 + \frac{q}{4} \right) \partial_r \psi = ik_0 \frac{q}{2} \psi \quad (3.6)$$

### Ground boundary condition

The ground boundary condition is held in the ground impedance  $Z$ , which is the ratio between the sound pressure and the normal particle velocity at  $z = 0$ .

$$Z = \frac{p_0}{v_{n,0}} = \frac{p_0}{\frac{1}{i\omega\rho_0} (\partial_z p)_{z=0}} \quad (3.7)$$

The derivative of  $p$  with respect to  $z$  is approximated to the second order and the ground boundary condition is written

$$Z = \frac{2i\omega\rho_{air}p_0\Delta z}{4p_{z=\Delta z} - 3p_{z=0} - p_{z=2\Delta z}} \quad (3.8)$$

where  $\Delta z$  is the discretization step in height.

### Upper boundary condition

The numerical domain is truncated at the top, eventually leading to sound waves reflected back into the calculation region. To block this phenomenon, the upper boundary condition is written as an absorbing layer at the top of the domain. In the implementation, it corresponds to an imaginary term added to the wave number

$$k(z_t < z < z_M) = k(z) + iA_t \frac{(z - z_t)^2}{(z_M - z_t)^2} \quad (3.9)$$

where  $A_t$  depends on frequency. The thickness and height of the absorbing layer should be chosen carefully, adequate to absorb the unwanted reflection but not the highest refracted sound rays.

## 3.2 Impedance model

### 3.2.1 Brief description of ground impedance

When solving the wave equation, the ground surface is usually taken into account by a mathematical boundary condition for the sound field above the ground surface. This condition contains the acoustic impedance of the ground surface as a parameter.

In the calculations, natural ground surfaces are modeled. They can be modeled as porous media. The acoustic impedance  $\zeta$  of a porous medium is defined as the ratio between the complex pressure and velocity amplitudes, for the case of a plane wave traveling in the medium. The normalized acoustic ground impedance is defined as  $Z = \frac{\zeta}{\rho_{air} \cdot c(z)}$ . It is the parameter governing the reflection of sound waves on a ground surface.

Several models for the normalized ground impedance have been developed. Delany and Bazley (1970) presented an empirical one-parameter impedance model for fibrous absorbing materials:

$$Z = 1 + 0.0511 \left( \frac{\sigma}{f} \right)^{0.75} + i \cdot 0.0768 \left( \frac{\sigma}{f} \right)^{0.73} \quad (3.10)$$

where  $\sigma$  is the ground flow resistivity, and  $f$  the frequency.

Attenborough (1992) developed various theoretical models for the acoustic impedance. The main one is a two-parameter model

$$Z = \frac{1 + i}{\sqrt{\pi \cdot \gamma_{air} \cdot \rho_{air}}} \sqrt{\frac{\sigma_e}{f}} + i \frac{c_0 \cdot \alpha_e}{8\pi \cdot \gamma_{air} \cdot f} \quad (3.11)$$

where  $\sigma_e$  and  $\alpha_e$  are the Attenborough parameters,  $\rho_{air}$  is the air density, and  $\gamma_{air}$  is the ratio of the air specific heats.

Figure 3.1 shows a comparison between the two models for the normalized ground impedance  $Z$ , in the case of thick grass ground and a harder ground.

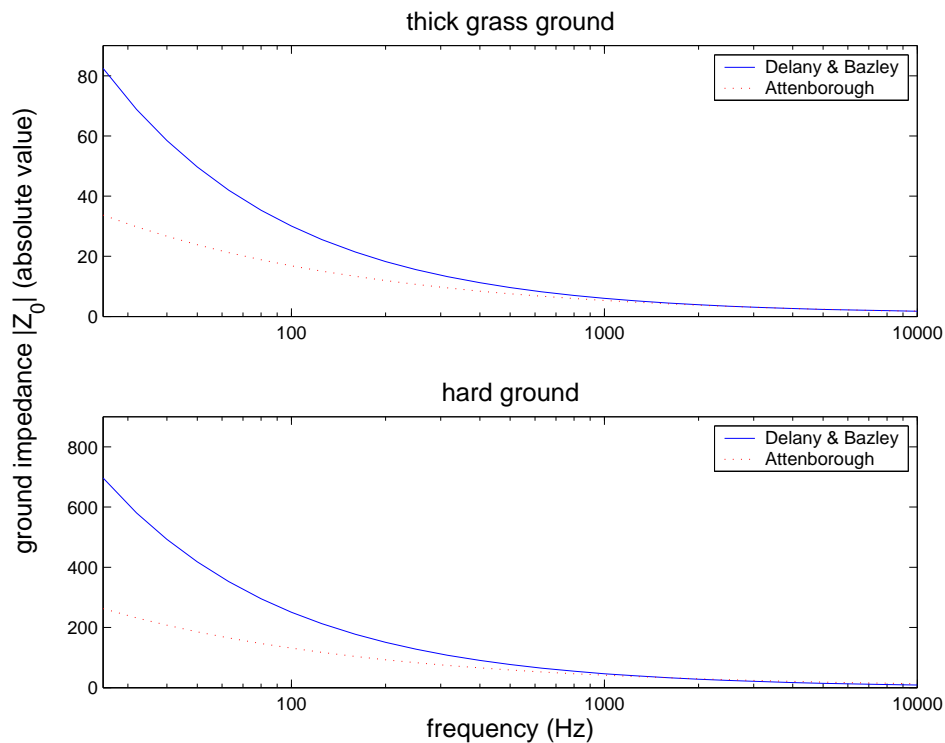


Figure 3.1: Absolute value of the normalized ground impedance for Delany&Bazley and Attenborough models over frequency, for two ground surfaces.

The figure shows considerable differences between the models, for the lowest frequencies. Above 1000 Hz, the two models agree fairly well.

### 3.2.2 Influence of ground impedance

However, it is important to note that the ground surface normally has its largest effect on the sound propagation for cases with long range propagation compared to the heights of the source and the receiver. Depending on the frequency range of interest, and on the geometry of the problem, the choice of a model for the normalized ground impedance may not be crucial.

Figure 3.2 shows this variable influence of the ground surface. Calculation is made for 100 Hz for which the impedance models significantly differ (see Figure 3.1).

For the case of a low source position compared to the propagation length (top figure), calculation with the two impedance models yields a difference up to 4 dB all along the propagation range. On the contrary, for the case of a higher source position (bottom figure), calculation with the two impedance models yields no difference all along the propagation range.

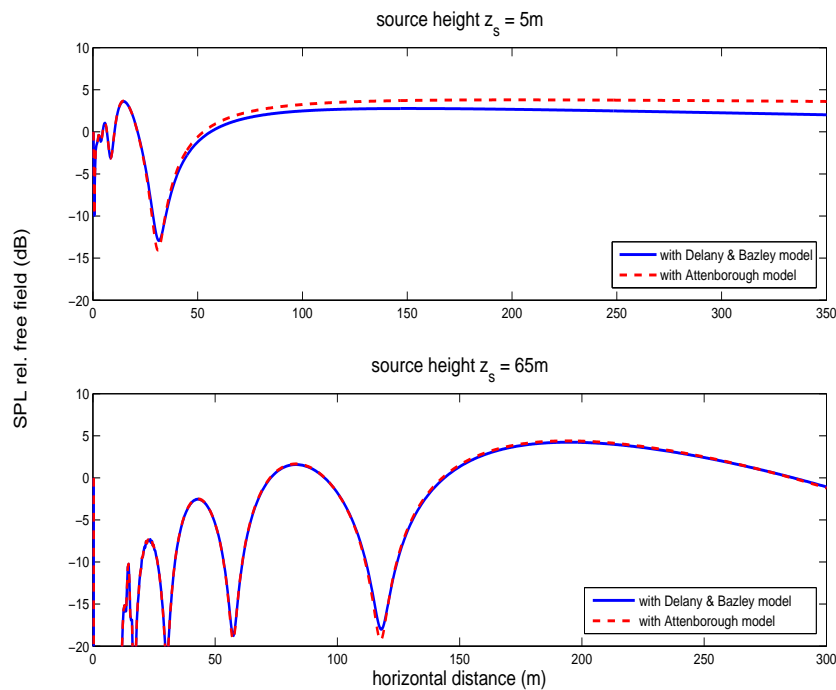


Figure 3.2: Sound pressure level relative to free field calculated with the two models for ground impedance. The source is at height  $z_s = 5$  m (top figure) and  $z_s = 65$  m (bottom figure). The receiver is at height  $z_r = 5$  m for both case. Calculation is made for 100 Hz.

### 3.3 Sound speed profile

The sound propagation model implemented earlier includes the effect of meteorological parameters by using the concept of effective sound speed (see Section 2.3.1). The sound speed is approximated with an analytical profile, either linear or logarithmic. It is then used to calculate the wave number  $k = \frac{\omega}{c_{eff}(z)}$ , the key parameter for the meteorological information.

#### 3.3.1 Linear profile

Linear profiles for effective sound speed follow the formulation below:

$$c_{eff}(z) = c_0(1 + az) \quad (3.12)$$

where  $c_0$  is a reference sound speed and  $a$  the refraction parameter.

The case  $a < 0$  corresponds to a negative gradient and the case  $a > 0$  corresponds to a positive gradient.

A linear profile is a first approximation of meteorological effects. However, it does not correspond to a realistic profile due to wind as it does not include the limit layer near the ground, and goes to infinity with increasing height.

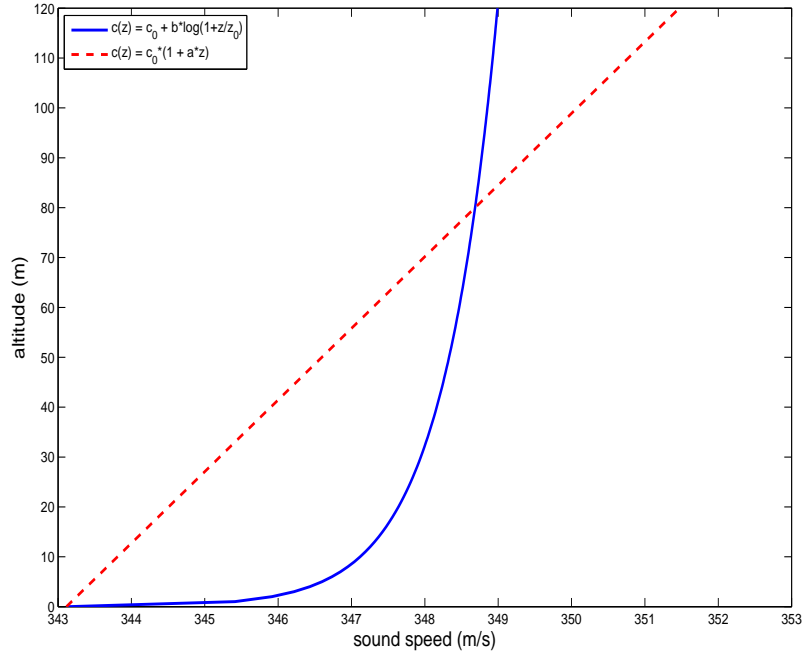


Figure 3.3: Linear and logarithmic profile for a ground sound speed  $c_0 = 343$  m/s. The profiles coefficients are set to  $a = 1.47 \cdot 10^{-4} \text{ m}^{-1}$ , and  $b = 1$  m/s,  $z_0 = 0.1$  m.

### 3.3.2 Logarithmic profile

Logarithmic profiles for effective sound speed follow the formulation below:

$$c_{eff}(z) = c_0 + b \ln \left( 1 + \frac{z}{z_0} \right) \quad (3.13)$$

where  $c_0$  is a reference sound speed,  $b$  the refraction parameter, and  $z_0$  the roughness length. The parameter  $b$  can be found from measuring the wind speed at a reference height.

$$b = \frac{v(z = z_{ref})}{\ln \left( \frac{z_{ref}}{z_0} \right)} \quad (3.14)$$

The roughness length  $z_0$  is a measure of the roughness of the surface over which the wind is blowing, defined as follows

$$z_0 = \frac{\epsilon}{30} \quad (3.15)$$

where  $\epsilon$  is the average height of surface irregularities (Auld and Srinivas 1995).

The logarithmic profile is widely used for sound propagation calculations as it constitutes a good approximation of the wind profile: important speed gradient near the ground which decreases rapidly with height.

### 3.4 Validation

The PE model implemented for outdoor sound propagation is to be validated. Comparisons are made between the model predictions of sound pressure level and alternative existing model predictions. For the validation, the geometry for which the sound propagation is calculated is fixed (see Figure 3.4). The varying parameters are:

- the wind, in terms of wind speed at 10 m high,
- the ground impedance, in terms of ground flow resistivity,
- the frequency.

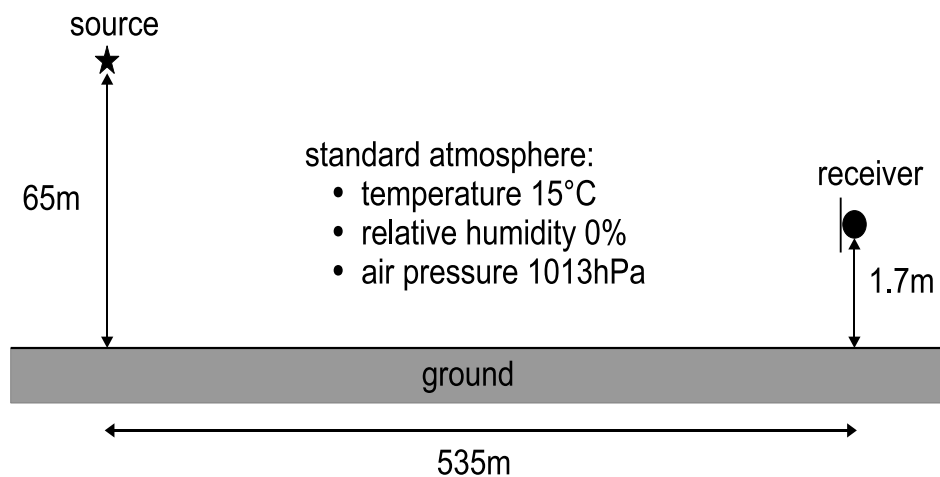


Figure 3.4: The figure shows the geometry used in the validation calculations for the PE propagation model.

For the whole validation section, the comparisons are made in terms of sound pressure levels relative to free field. The results are presented either as 2D-plots or as 1D-plots. For the 2D-plots, the sound pressure level is plotted for the entire domain for which the calculation is made. For the 1D-plots, the sound pressure level is plotted as a function of range at the receiver height  $z_r = 1.7$  m.

### 3.4.1 Comparison to analytical solution

The Helmholtz wave equation, Equation (2.2), can be analytically solved if the sound speed  $c$  (or the wave number  $k$ ) is constant in space. This is achieved if no wind profile is set in the calculation, i.e. the wind speed is 0 at 10 m for the logarithmic profile. In such a configuration, the PE model calculates the analytical solution. The comparison between the PE prediction and the analytical solution is made for two frequencies,  $f = 70$  Hz and  $f = 700$  Hz.

Figure 3.5 shows the comparison between the PE prediction and the analytical solution for the entire calculation domain at  $f = 70$  Hz.

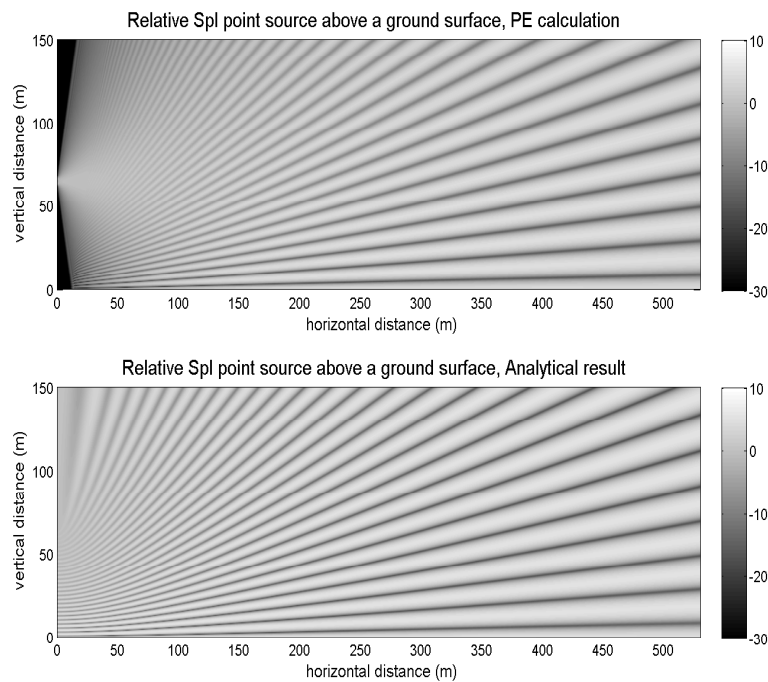


Figure 3.5: Comparison to analytical solution -  $f = 70$  Hz - Sound pressure level relative to free field plotted for the entire domain,  $Z_{max} = 150$  m,  $R_{max} = 535$  m.

Figure 3.5 shows a good agreement between the PE calculation and the analytical solution. One can notice that the PE calculation is valid for far field and for a limited elevation angle only, as the first hundred meters disagree.

$$\begin{aligned}
 \text{far field limitation} &\Rightarrow R \gg \frac{1}{k_0} = \frac{c_0}{2\pi \cdot f} \approx 0.8m \\
 \text{elevation angle limitation} &\Rightarrow R \geq \frac{z_s - z_r}{\tan(\beta)} \approx 135m \quad \text{for } \beta = 25^\circ
 \end{aligned} \tag{3.16}$$

Figure 3.6 shows the comparison between the PE prediction and the analytical solution at the receiver height at  $f = 70$  Hz.

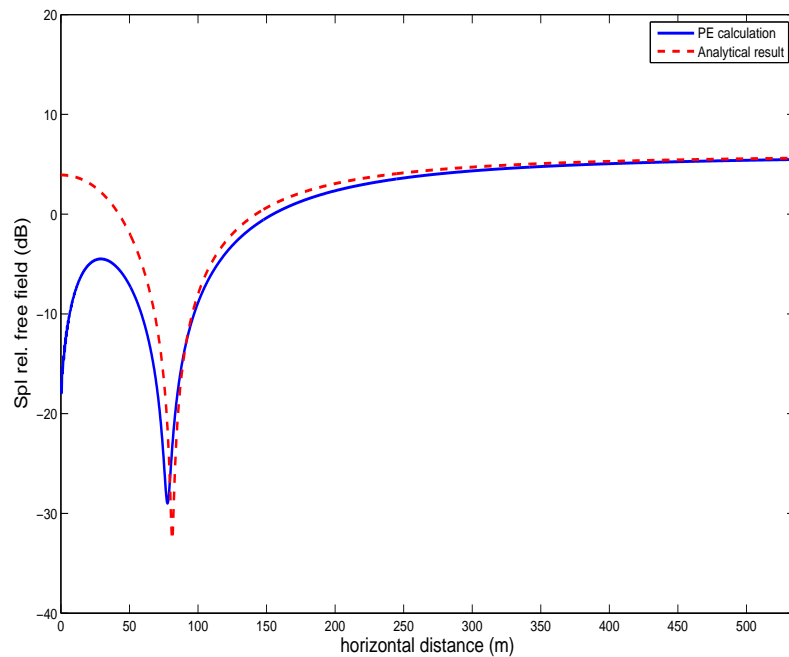


Figure 3.6: Comparison to analytical solution -  $f = 70$  Hz - Sound pressure level relative to free field plotted as a function of range at the receiver height,  $h_r = 1.7$  m.

Figure 3.6 shows again a good agreement in the distance range where the PE is valid. The discrepancy between the PE calculation and the analytical solution is at the most about 1 dB for ranges higher than 135 m (see Equation (3.16)).

Figures 3.7 and 3.8 show the similar comparisons between the PE prediction and the analytical solution at  $f = 700$  Hz. The conclusions are the same as for the validation made at  $f = 70$  Hz.

### 3.4.2 Comparison to a FFP calculation

For a propagation in inhomogeneous atmosphere, a comparison can be made between the PE prediction and the FFP prediction. A wind profile is fixed, i.e. a logarithmic profile is used with wind speed 5 m/s at 10 m height and roughness length 0.05 m. Again, the calculations are made for  $f = 70$  Hz and  $f = 700$  Hz.

Figure 3.9 shows the comparison between PE model and FFP model at  $f = 70$  Hz. Figure 3.10 shows the case at  $f = 700$  Hz. For both frequencies, the discrepancy between the PE calculation and the analytical solution is at the most about 1.5 dB at longer ranges.

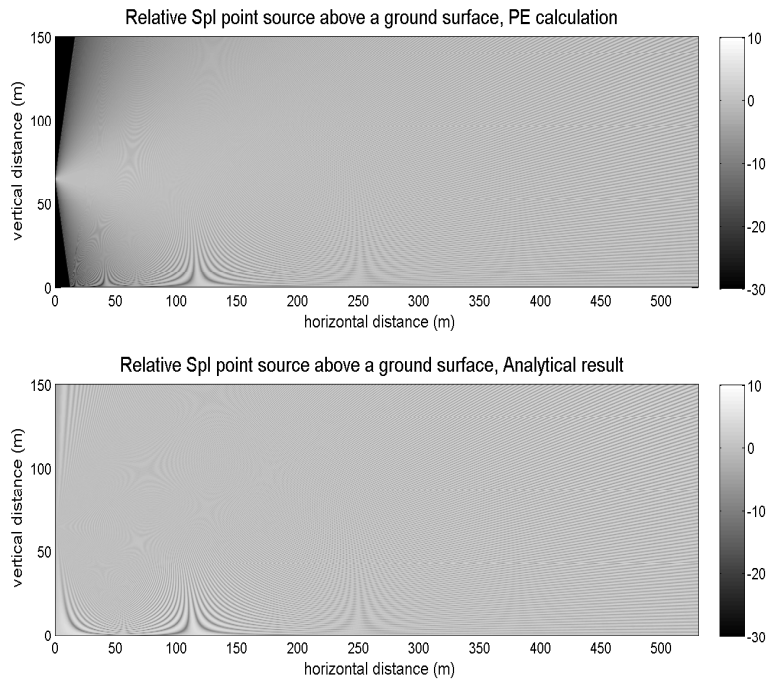


Figure 3.7: Comparison to analytical solution -  $f = 700$  Hz - Sound pressure level relative to free field plotted for the entire domain,  $Z_{max} = 150$  m,  $R_{max} = 535$  m.

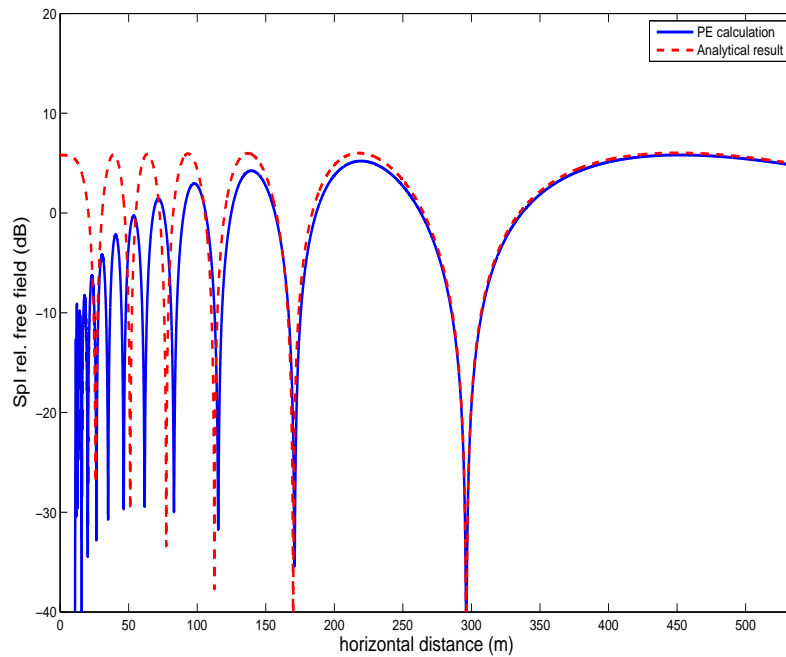


Figure 3.8: Comparison to analytical solution -  $f = 700$  Hz - Sound pressure level relative to free field plotted as a function of range at the receiver height,  $h_r = 1.7$  m.

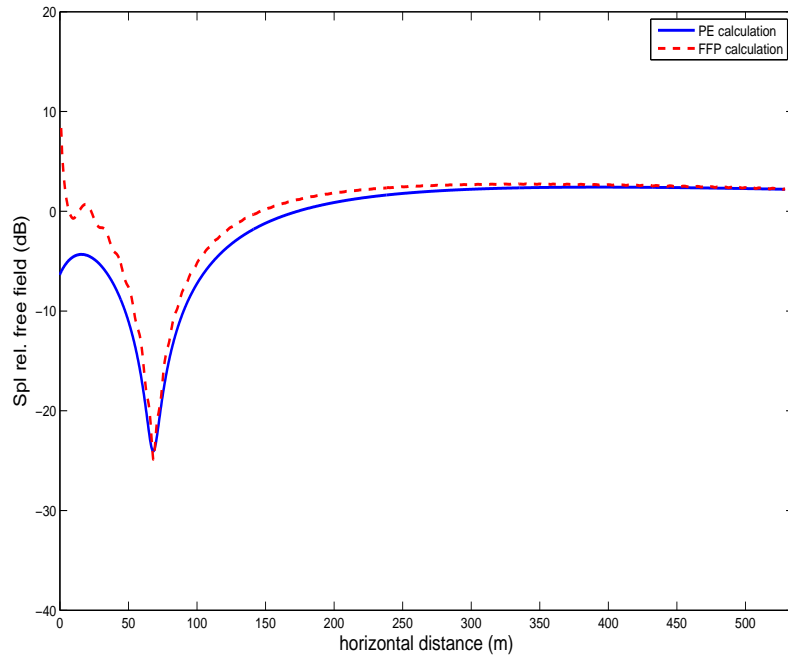


Figure 3.9: Comparison to FFP calculation -  $f = 70$  Hz - Sound pressure level relative to free field plotted as a function of range at the receiver height,  $h_r = 1.7$  m.

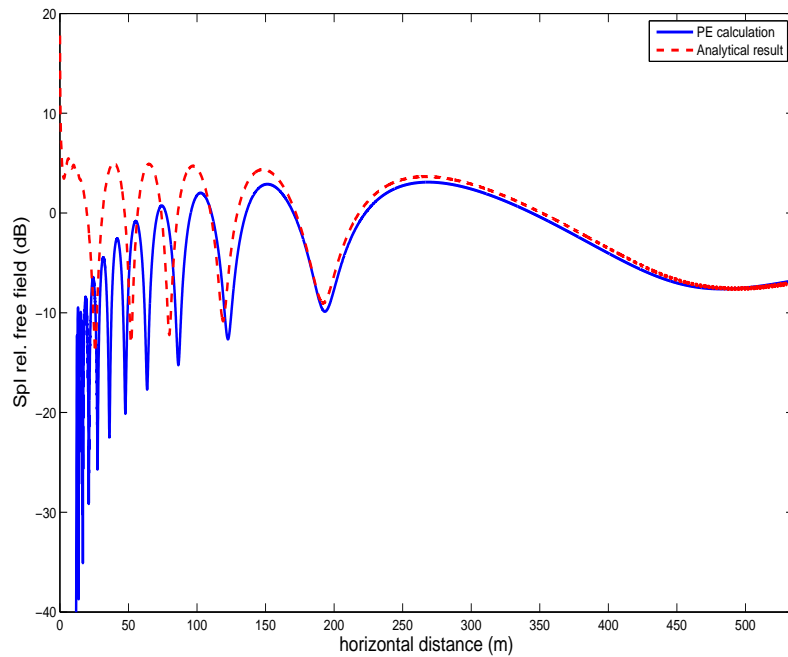


Figure 3.10: Comparison to FFP calculation -  $f = 700$  Hz - Sound pressure level relative to free field plotted as a function of range at the receiver height,  $h_r = 1.7$  m.

# Chapter 4

## Measurements

---

In the previous chapter, an outdoor sound propagation model was defined in order to accurately predict wind turbine noise propagation. This model includes all major outdoor effects which can influence sound propagation. A measurement campaign is undertaken in order to provide a realistic set of atmospheric conditions and sound pressure levels. The measurements are used to feed the model and predict immission levels. This chapter presents the measurement campaign.

---

### 4.1 Introduction

The measurements were carried out during the autumn 2005, in Skåne, southern Sweden. The measured data consisted of both sound and meteorological data.

The sound data comprised of 10 minute long recordings of the wind turbine noise, on a regular basis. It was acquired approximately 530 m away from the turbine. In parallel to acoustic measurements, a number of parameters were monitored, such as wind speed and direction, temperature and other atmospheric parameters, as well as produced electric power and Revolutions Per Minute.

In total, more than 700 measurements were taken at wind speeds up to 18 m/s (at the standard height of 10 m).

### 4.2 Test set-up

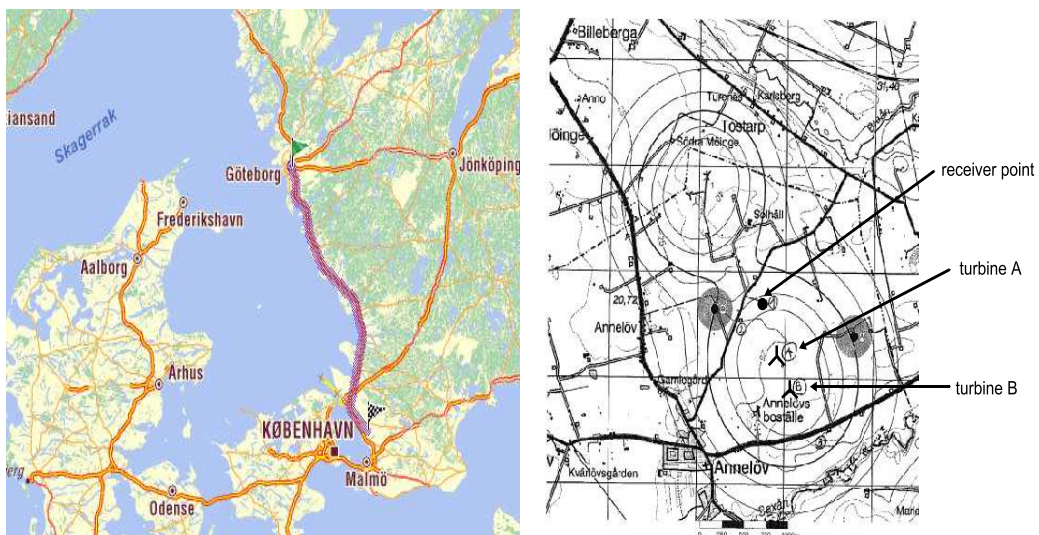
#### 4.2.1 Measurement site

Acoustic and meteorological measurements were simultaneously carried out in November-December 2005, in Annelöv, Skåne, Sweden (300 km south of Göteborg). The site was a typical agricultural area with very few obstacles (trees, bushes, buildings). The measurement set-up was situated on soft ground, at a dwelling located to the south of the wind turbine at a distance of about 550 m. The topography of the terrain was very flat. The ground was cultivated during the first measurement days. It was covered with snow during the last measurement days. Few roads were in the vicinity of the measurement point, with hardly any car traffic.

The site comprised actually two wind turbines, which were 290 m apart. The measurement set-up was located in alignment with the wind turbines.



Figure 4.1: Measurement site with two wind turbines and measurement set-up.



(a) Denmark and southern Sweden. Both Göteborg and Annelöv are pointed out. (b) The Annelöv site with 2 wind turbines and receiver point, roads and dwellings.

Figure 4.2: Location of wind turbine 715, Annevind 2

The measurements were carried out on a three-bladed wind turbine, Enercon E66, which has a rotor diameter of 70 m, and a hub height of 65 m (Figure 4.1). Its nominal power is 1.5 MW. On the official Swedish list of wind turbines, it corresponds to the wind turbine number 715, Annevind 2. The field where the wind turbine was put up is owned by Bengt Hellerström, Annlövs boställe. The wind turbine itself is owned by Ekovind AB (Drottninggatan 3, 447 35 Vårgåda).

The measurements were performed outdoors, and the measurement equipment was set-up in a caravan, parked in front of two farm buildings.

### 4.2.2 Acoustic measurements and equipment

Immission measurements were carried out by following as closely as possible the recommendations provided in Ljunggren (1997).

The acoustic data was recorded, for 10 minutes every hour, 24 hours a day for 30 days, from November, 16<sup>th</sup> to December, 15<sup>th</sup>. A Matlab program, developed by the author, started the recordings and saved the sound data as wave files. The wave files were acquired at a sampling frequency of 44.1 kHz.

The acoustical data was recorded using a microphone, mounted at the center of a vertical square wooden board of 1 m<sup>2</sup>, attached to the long side of the caravan. The microphone was positioned so that the membrane plane was orthogonal to the platform. It was equipped with a primary and secondary windscreen, with diameter 7 cm and 40 cm, respectively. The measured values of sound levels were in the analysis reduced by 6 dB due to pressure doubling. The microphone was positioned 534 m away from the turbine, at a height of 1.7 m.

The microphone used for the measurements was a Bruel&Kjaer microphone  $\frac{1}{2}$  inch type 4165, coupled with a Bruel&Kjaer preamplifier type 2669. Recordings were done for frequencies from 50 to 20000 Hz and sound pressure levels from 6 to 96 dB.

The frequency response and directivity of the B&K microphone were taken from the document "Product Data - Condenser Microphone Cartridges - Types 4133 to 4181", B&K webpage (<http://www.bksv.com/pdf/Bp0100.pdf>). It showed a flat response (variation <1 dB) for frequencies up to 10 kHz. No corrections were applied for the microphone directivity since the document showed that these effects amounted for less than 1.5 dB up to 6 kHz, for all angles of incidence. Moreover, these effects are the same for all measurements.

Before the measurements, the sensitivity at 1 kHz was determined for the microphone using a calibrated pistonphone. This recorded signal was saved as it gives the calibration factor needed for post-processing the recorded data.

The measurement chain was kept intact during the entire measurement series.

### 4.2.3 Meteorological measurements and equipment

At the measuring point (caravan), a meteorological mast was equipped with sensors for wind speed and wind direction, temperature and relative humidity, and atmospheric pressure. The sensors were coupled to a weather station which saved the measured values. Wind speed and direction were measured at 10 m height. Temperature and relative humidity were measured at 10 m and 2 m height. Atmospheric pressure was measured with an anemometer included in the weather station. An extra measurement of temperature was made at the wind turbine, at

the hub height (65 m) and at 10 cm above ground.

The weather station used for the measurements was the ELV WS 2500 Touch-Screen semiprofessional weather station. The wind speed and direction were measured with a speed and direction wind sensor S 2000 W-1. The temperature and relative humidity were measured with a temperature/humidity sensor S 2001 A. The resolution of the instruments was 0.1 m/s for wind speed, 5° for wind direction, 0.1 °C for temperature, and 1% for relative humidity. The internal anemometer had a resolution of 1 hPa. Finally, the temperature/humidity sensor used at 65 m height was a Tinytag Plus RH with a resolution of 0.01 °C for the temperature and 0.5% for the relative humidity. The accuracy of the instruments was  $\pm 2\%$  at 8 m/s for wind speed,  $\pm 1\text{ °C}$  for temperature,  $\pm 8\%$  for relative humidity,  $\pm 1\text{ hPa}$  for the internal anemometer. Finally, the Tinytag Plus RH had an accuracy of  $\pm 3\%$  at 25 °C.

In addition to those measurements, the wind speed at the hub height and the blades Revolution Per Minute (rpm) were collected by Vattenfall AB, who is responsible for the official wind power statistics in Sweden. Data was transferred from the hub into an Excel data file by calling up the computer system regulating the wind turbine.

The meteorological data, acquired through the weather station, was automatically downloaded every 15 minutes. The meteorological data provided by Vattenfall AB consisted of 10 minutes averages. The start of the acoustic measurements was synchronized each hour with the hub and weather station meteorological data.

A list of of the meteorological sensors and heights are given in Table 4.1.

Table 4.1: *Meteorological equipment and measuring positions ( $t$  = temperature (°C),  $ws$  = wind speed (m/s),  $wd$  = wind direction (°),  $rh$  = relative humidity,  $p_{atm}$  = atmospheric pressure (hPa))*

Height (m)	Parameter	Equipment
0.1	$t, p_{atm}$	Tinytag Plus RH, weather station internal anemometer
2	$t, rh$	temperature/humidity sensor S 2001 A
10	$t, rh, ws, wd$	temperature/humidity sensor S 2001 A, wind sensor S 2000 W-1
65	$t, rh$	Tinytag Plus RH

### 4.3 Data processing

The sound data comprises of recorded signal. For each recording, the main aim is to know the total, A-weighted sound pressure level.

### 4.3.1 Calibration

The first step of data processing is the calibration of the recorded signals. As mentioned in Section 4.2.2, the microphone was calibrated before the measurements started and the calibration signal was saved. This signal is used to scale all the recorded sound signals to true values.

### 4.3.2 Extraction of the frequency content

The Matlab spectrogram tool is used to extract the frequency content of the recorded signals. The spectrogram is the result of calculating the frequency spectrum of a time signal. It is a three-dimensional plot of the energy of the frequency content of a signal as it changes over time.

Spectrograms are usually calculated from the time signal using the short-time Fourier transform (STFT). Digitally sampled data, in the time domain, is broken up into overlapping segments and Fourier transformed to calculate the magnitude of the frequency spectrum for each segment. Each segment corresponds to an estimate of the short-term, time-localized frequency content of the signal.

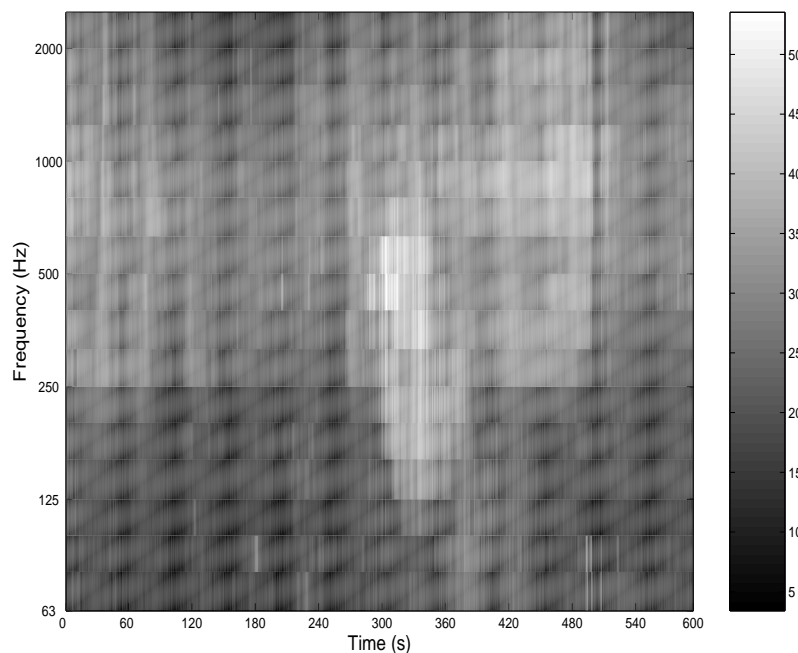


Figure 4.3: A spectrogram of a recorded signal with frequency on the vertical axis and time on the horizontal axis.

For this case, the spectrogram tool calculates the acoustic pressure magnitude for short time intervals.

### 4.3.3 Determination of sound pressure levels

The acoustic pressure values which were calculated with the spectrogram tool are summed up over the recording time interval, within the 18 standardized  $\frac{1}{3}$ -octave bands from 50 to 2500Hz. Tests by trial and error showed that adding those frequency bands was sufficient. The results are obtained in terms of A-weighted sound pressure levels as function of frequency,  $L_P(A)_i, i = 1 \dots N$ . The total, A-weighted sound pressure levels are also estimated, based on the formulation

$$Lp(A)_{tot} = 10 \log \left( \sum_{i=1}^{i=N} 10^{L_P(A)_i/10} \right) \quad (4.1)$$

## 4.4 Conclusion

After the measurement campaign, about 720 wind turbine noise measurements, and associated weather data, are available as input data for the model. They correspond to situations with many different meteorological conditions:

- wind speeds varying from 0 to 18 m/s, with different directions,
- a temperature gradient range from -0.25 to +0.30 °C/m,
- a wide range of other atmospheric parameters.

The measurements carried out are promising. Comparisons between the measurements and the models calculations are possible, which will hopefully lead to a good validation of the designed model.

# Chapter 5

## Analysis and results

---

This chapter presents the analysis of the measurements. The first part gets onto the assessment of the source output sound power and the background noise issue. It develops how the acoustic and meteorological data was selected and statistically treated. The second part of this chapter presents the results from the measurements. First, the measured sound pressure levels are related to the sound propagation conditions with special emphasis on meteorological conditions. Also, the measured sound pressure levels are compared to the Swedish standard and PE predictions in focus.

---

### 5.1 Analysis

#### 5.1.1 Estimation of the source output sound power

The source output sound power was needed as an input parameter for both the calculations according to the standard and the PE model. An estimation of the sound power level as a function of the blades rotations per mminute  $rpm$  is given in van den Berg (2003),

$$L_W(A) = 67.1 \log(rpm) + 15.4 \text{ dBA} \quad (5.1)$$

where  $L_W(A)$  is the sound power level in dBA.

This regression was derived from measurements made at a wind turbine of the same model as the one in this study. Moreover, they were performed for  $rpm$  from 10 to 22. Hence, this output sound power estimation can only be assumed to be valid in this range.

The rotational speed relates to the wind speed at hub height (65 m). With the hub data collected from Vattenfall, it is possible to link the rotational speed to the wind speed at the hub height.

In Figure 5.1, the blades  $rpm$  is plotted as a function of wind speed at hub height  $u_{65}$ . The best fit to the data points is

$$rpm = -0.013u_{65}^3 + 0.28u_{65}^2 + 0.37u_{65} + 8.5 \quad (5.2)$$

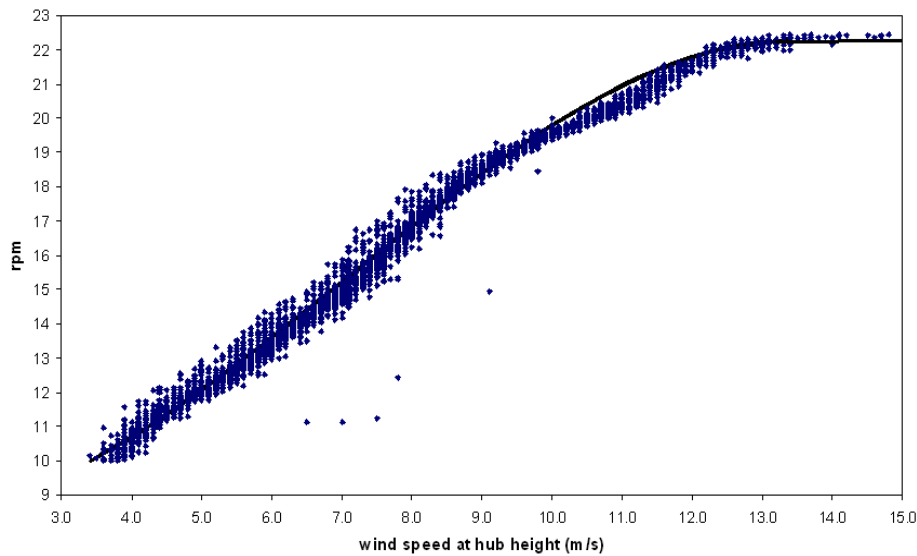


Figure 5.1: Blades rotations per minute as a function of wind speed measured at hub height (65 m). Also drawn is the best fit to the data points.

with a correlation coefficient of 0.99. The *rpm* is constant, at a value of 22.5, for wind speeds higher than 13.5 m/s.

However, wind turbine noise measurements are usually presented as a function of wind speed at the reference height 10 m. An estimate of the wind speed at 10 m is calculated from a logarithmic profile and the wind speed measurement at 65 m.

$$u_{10} = \frac{u_{65}}{\ln \frac{65m}{z_0}} \ln \left( 1 + \frac{10m}{z_0} \right) \quad (5.3)$$

where  $z_0 = 0.05$  m is the ground roughness length.

With the last three relations (Equation (5.1), (5.2) and (5.3)), it is possible to estimate the output sound power level of the wind turbine from a wind speed at 10m, assuming that  $u_{65}$  is unaffected by the wind turbine and that the wind profile is really logarithmic.

The wind speed at 10 m,  $u_{10}$ , is needed for the comparison between the measurements and the predictions. An alternative approach to find  $u_{10}$  would be to make a best fit between measured  $u_{10}$  at the range of the receiver and  $u_{65}$ . This approach, however, was concluded to lead to larger errors.

### 5.1.2 Estimation of the background noise

For the two models predictions, one unique noise source was assumed: the generation of noise by the wind turbine rotating blades. In the measurements, the sound

pressure levels also included background noise. An important task was thus to assess the influence of the background noise on the measured levels.

The background noise is the total of all noise sources, excluding the noise from the wind turbine under consideration, at the time of the measurements. Ambient noise constitutes part of the background noise: it consists of the existing environmental sound such as human or animal activity, or action of the wind through foliage and around obstacles close to the measurement location. Other sources of background noise can be noise generated by wind at the microphone diaphragm or electric noise in the instrumentation.

The safest way to take the background noise into account is to disregard any measurement for which the sound pressure level is not at least 6 dB higher than the background level. This criterion is used here. By doing so, assuming that the background noise levels have no influence on the measured levels leads to an error  $\leq 1$  dB.

$$\begin{aligned}
 Lp_{windturbine} &= AdB \\
 Lp_{backgroundnoise} &= A - 6dB \\
 \implies Lp_{resulting} &= 10 \log \left[ 10^{\frac{A}{10}} + 10^{\frac{A-6}{10}} \right] \\
 &= 10 \log \left[ 10^{\frac{A}{10}} * \left( 1 + 10^{-\frac{6}{10}} \right) \right] \\
 &= 10 \log \left[ 10^{\frac{A}{10}} \right] + 10 \log \left[ 1 + 10^{-0.6} \right] \\
 &= A + 0.97dB
 \end{aligned} \tag{5.4}$$

According to Ljunggren (1997), the background noise should be measured with the turbine parked immediately before or after the measurement of the turbine noise at the measurement points. This recommendation could not be followed but a background noise measurement can be defined as a recording performed when the noise source is turned off, thus when the two wind turbines are not running. Such recordings should be sufficient to provide reliable assessment of the background noise level.

Situations during which both wind turbines were turned off occurred 14 times, at occasions when the wind speed was too low for the blades to rotate. The background noise was estimated to 18dB(A) for low wind speeds.

An interesting question is to determine whether the background noise level was dependent on the wind speed. Situations during which the wind turbines were turned off, at occasions with varying wind speeds, occurred 3 times. For those recordings, the wind speeds were of 11.2-14 m/s and the background noise was estimated to 35.3-40.6 dB(A).

By extrapolation of these data to intermediate wind speeds, the criterion used for not disregarding data - a difference of 6 dB between measured values and back-

ground noise - can be seen to hold.

### 5.1.3 Selection of the data

#### Selection of eligible meteorological data

For the last measurement day (15<sup>th</sup> of December), the temperature data at the wind turbine was not available. This renders the recordings incomparable to the PE calculations.

The estimation of the source output power was not possible for *rpm* lower than 10 (see Section 5.1.1), thus for wind speeds lower than 2.6 m/s at 10 m. All data recorded with wind conditions lower than this limit can not be used for the calculations.

Finally, the last meteorological inclusion criterium is the wind direction. The aim is to consider true downwind or upwind propagations. As a consequence, only recordings for which the wind directions were within an angle  $\pm 45^\circ$  from the wind turbine - microphone direction are considered.

#### Selection of eligible sound data

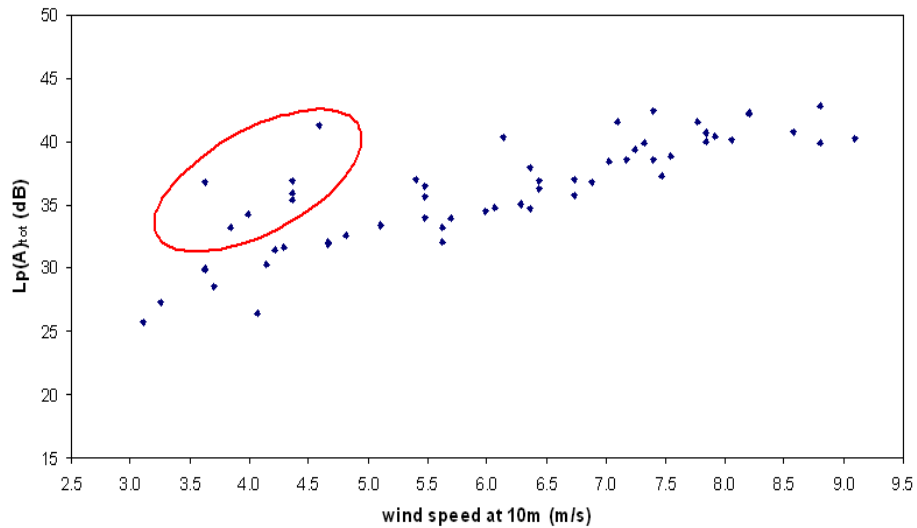
After exclusion of illegible meteorological data, only 140 recordings remained. In Figure 5.2, those measurements are plotted as a function of wind speed at 10 m. Downwind and upwind propagation cases are plotted apart.

Some values of sound pressure levels, especially for low wind speeds, are surprisingly high. Those recordings were investigated more closely in order to find explanations for the high values of sound pressure levels. A study of the spectrograms of all data points circled in Figure 5.2 showed particular events which made the levels unexpectedly high. A listening of the corresponding recordings showed that the contamination of recordings was caused by phenomena as various as road traffic noise, tractor noise, radio playing, dogs barking, and airplane noise. Recordings identified as being polluted by noises other than from the wind turbines are hence omitted.

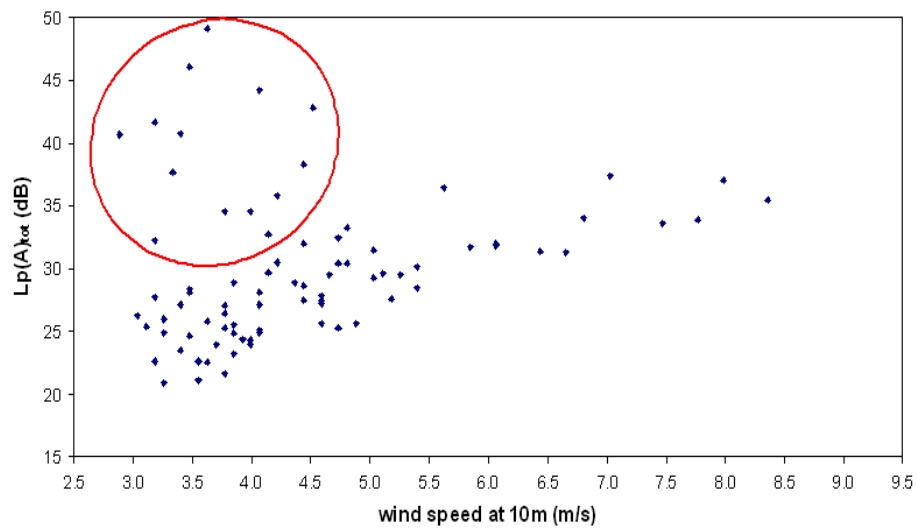
### 5.1.4 Statistical treatment of the data

In the following (Section 5.2), the relation between the sound pressure levels and the weather conditions is described through a regression technique. The regression lines are fitted using the standard least squares regression. Two assumptions underlie the method:

- the values of the outcome variable (sound pressure levels  $L_P(A)_{tot}$ ) should



(a) Downwind propagation



(b) Upwind propagation

Figure 5.2: Recorded equivalent A-weighted sound pressure levels plotted as a function of wind speed at 10 m for downwind and upwind propagation conditions. The polluted values are circled.

have a Normal distribution for each value of the predictor variable (variable for weather conditions);

- the variability of the outcome variable, as assessed by the variance or standard deviation, should be the same for each value of the predictor;

The uncertainty of the regression line is estimated by the 95% confidence interval. It is calculated with the auto- and cross-correlations of the predictor and outcome variables.

The statistical calculations are made according to the mathematical formulation given in Altman (1991) and described in Appendix C.

## 5.2 Results

### 5.2.1 Measurements

The measured total, A-weighted sound pressure levels are computed and plotted as a function of wind speed at 10 m height (Figure 5.3) and temperature gradient (Figure 5.4).

The temperature gradient chosen for the results analysis is the temperature difference divided by the height difference, in °C/m or K/m, between the measurements at 10 m and at 2 m.

$$\Delta T = \frac{T_{10m} - T_{2m}}{8} \quad (5.5)$$

In the following, only the selected data points (see Section 5.1.3) are used. The plots show downwind propagation only.

Figure 5.3 shows the measured total, A-weighted sound pressure levels as a function of the wind speed at 10 m height.

Figure 5.3 shows a clear trend: the total, A-weighted sound pressure level increases with the wind speed at 10 m. A linear trend line is fitted to the measurements,

$$L_P(A)_{tot} = 2.5u_{10} + 20.1 \quad (5.6)$$

with a correlation coefficient of 0.89. The confidence interval at 95% is also drawn.

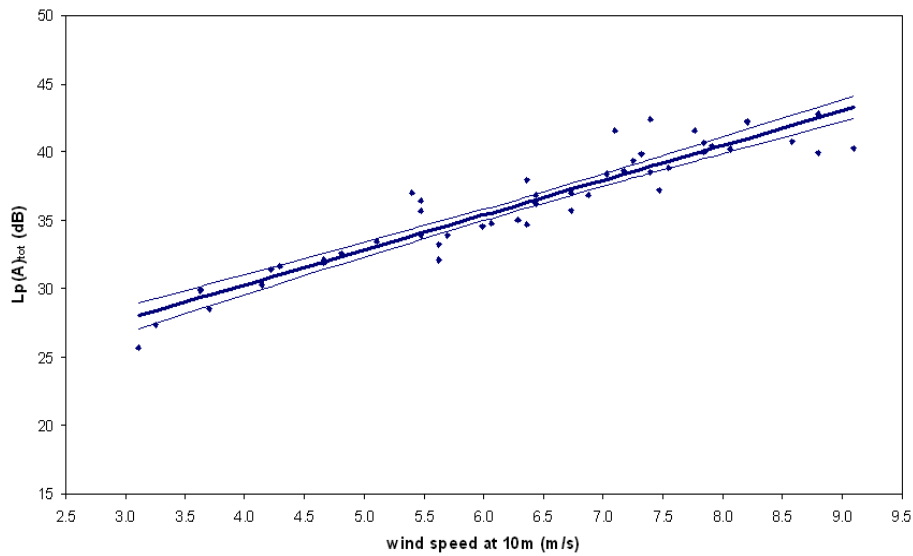


Figure 5.3: Measured total, A-weighted sound pressure levels as a function of wind speed at 10 m. The best fit to the data points and the confidence interval at 95 % are also drawn.

Figure 5.4 shows the measured total, A-weighted sound pressure levels as a function of the temperature gradient, with no concerns about the wind speed.

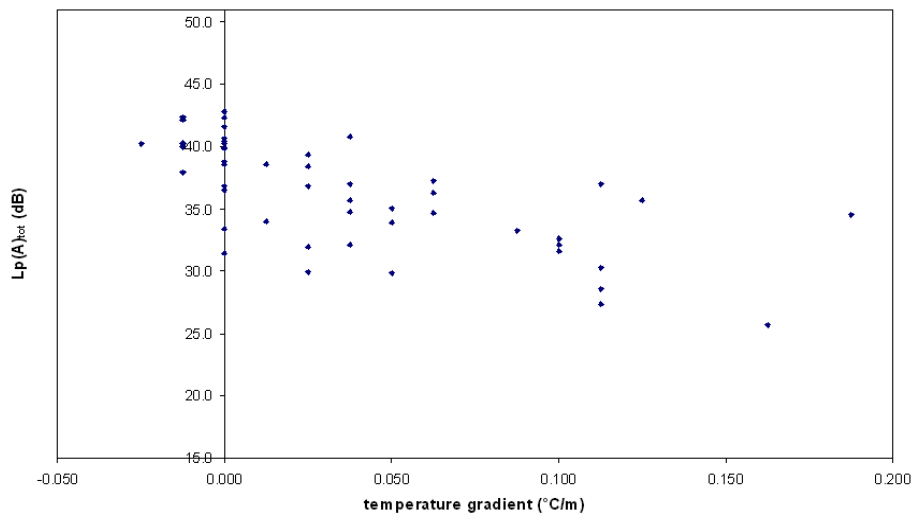


Figure 5.4: Measured total, A-weighted sound pressure levels as a function of temperature gradient.

It shows that the data points are much more spread, with no clear trend. However, the influence of the temperature gradient on the measured sound pressure levels is likely to be more noticeable when the influence of the wind speed is not too important, which is the case for lower wind speeds (for example, under 5 m/s at 10 m height).

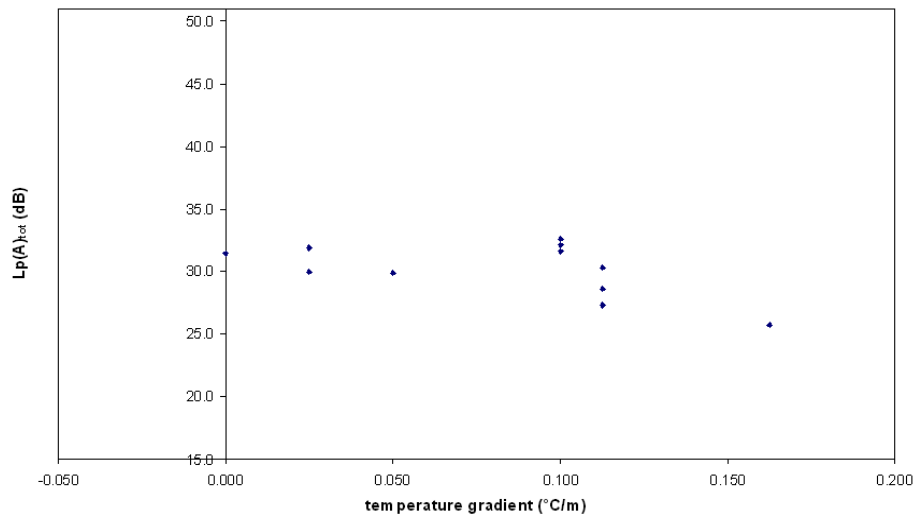


Figure 5.5: Measured total, A-weighted sound pressure levels as a function of temperature gradient, for low wind speeds (3-5 m/s) at 10 m.

Figure 5.5 shows the measured total, A-weighted sound pressure levels as a function of the temperature gradient for wind speeds from 3 to 5 m/s.

No evident trend is visible. In addition, the very few number of data points implies that no conclusions can be drawn from this data.

## 5.2.2 Swedish standard calculations

As mentioned in Section 2.4.1, the standard calculates one single value for a specified weather situation (supposedly a worst case). However, in order to estimate how the standard performs, it is more self-explanatory to compare the calculated sound pressure levels to the measured ones for the whole range of wind speeds relevant for the measurements. Thus, the total, A-weighted sound pressure levels are calculated based on the standard formula (see Equation (2.11)), and the power level formula (see Equation (5.1)).

Again, the measured total, A-weighted sound pressure levels, as well as the standard calculations are plotted as a function of wind speed at 10 m in Figure 5.6. A linear trend line is fitted for both set of data points,

$$\begin{aligned}
 \text{measured } L_P(A)_{tot} : & \quad L_P(A)_{tot} = 2.5u_{10} + 20.1 \\
 \text{standard } L_P(A)_{tot} : & \quad L_P(A)_{tot} = 3.0u_{10} + 11.4
 \end{aligned} \tag{5.7}$$

with correlation coefficients exceeding 0.89. The confidence interval at 95% is drawn for both sets of data points.

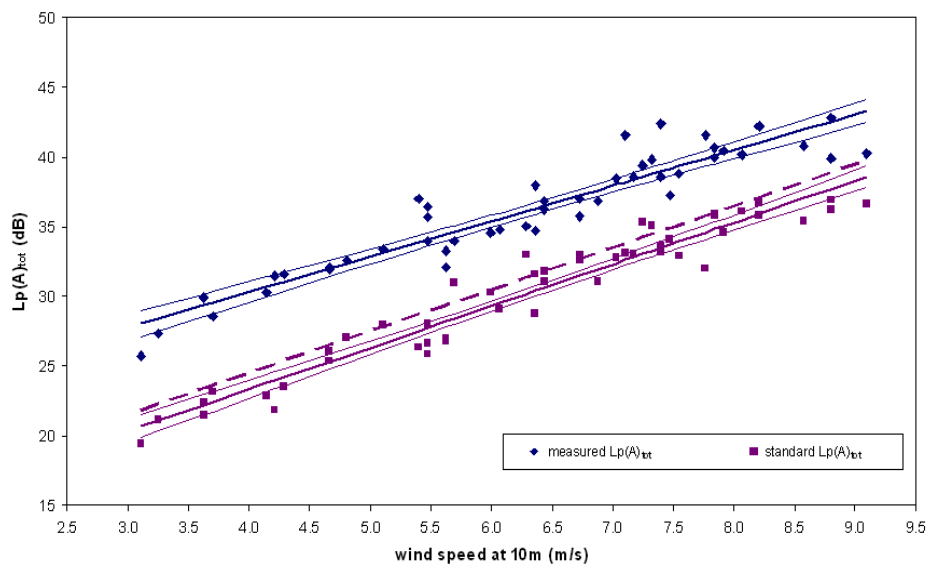


Figure 5.6: Standard calculated total, A-weighted sound pressure levels compared to the measured total, A-weighted sound pressure levels. The best fit and confidence interval at 95% for both sets are also drawn. The dashed line corresponds to an estimated increase of SPL due to the contribution of the second wind turbines.

For the measured wind speed range, the standard calculations deviate from the measured levels. The confidence intervals at 95% for the measured and standard calculated  $L_P(A)_{tot}$  do not overlap. This confirms that the standard significantly differs from the measurements. The deviation of the standard from the measurements ranges from 5 to 7 dB.

The presence on site of the second wind turbine 290 m further away (see Section 4.2.1) corresponds to an increase of the total, A-weighted sound pressure levels of 1.2 dB. The dashed line in Figure 5.6 corresponds the resulting total, A-weighted sound pressure levels as a function of wind speed at 10 m.

### 5.2.3 PE calculations

#### Results

As stated in Section 2.4.3, the important computational time necessary to the PE calculations is the major limit to the test of this sound propagation model. As a consequence, not all the measurements can be compared to a calculated PE level. Measurements were selected, after listening, regularly within the range of measured wind speeds at 10 m. The total, A-weighted sound pressure levels were calculated with the PE model, using the corresponding measured meteorological parameters.

Table 5.1 gives the list of the meteorological parameters corresponding to the 12 chosen measurements along the range of measured wind speeds at 10 m.

Table 5.1: Selected measurements and meteorological parameters, used as input parameters for the PE predictions.

Wind speed (m/s)	<i>rpm</i> (/min)	Temperature gradient (°C/m)	Relative humidity (%)	Air pressure (hPa)
3.3	11.5	+0.1125	88	1008
3.7	12.0	+0.1125	84	1008
4.1	12.7	+0.1125	83	1008
4.7	13.3	+0.1000	88	1027
5.5	13.7	+0.0125	87	1015
6.0	16.0	+0.1875	83	1007
6.4	14.9	-0.0125	87	990
6.7	17.0	+0.0375	79	1005
7.2	17.2	+0.0000	88	1000
7.8	19.0	+0.0125	83	997
8.6	18.7	+0.0375	74	986
9.1	19.5	+0.0000	84	988

The measured total, A-weighted sound pressure levels, as well as the PE calculations are plotted as a function of wind speed at 10 m in Figure 5.7. A linear trend line is fitted for both set of data points,

$$\begin{aligned}
 \text{measured } L_P(A)_{tot} : \quad & L_P(A)_{tot} = 2.5u_{10} + 20.1 \\
 \text{PE } L_P(A)_{tot} : \quad & L_P(A)_{tot} = 2.8u_{10} + 10.3
 \end{aligned}
 \tag{5.8}$$

with correlation coefficients exceeding 0.89. The confidence interval at 95% is drawn for both sets of data points.

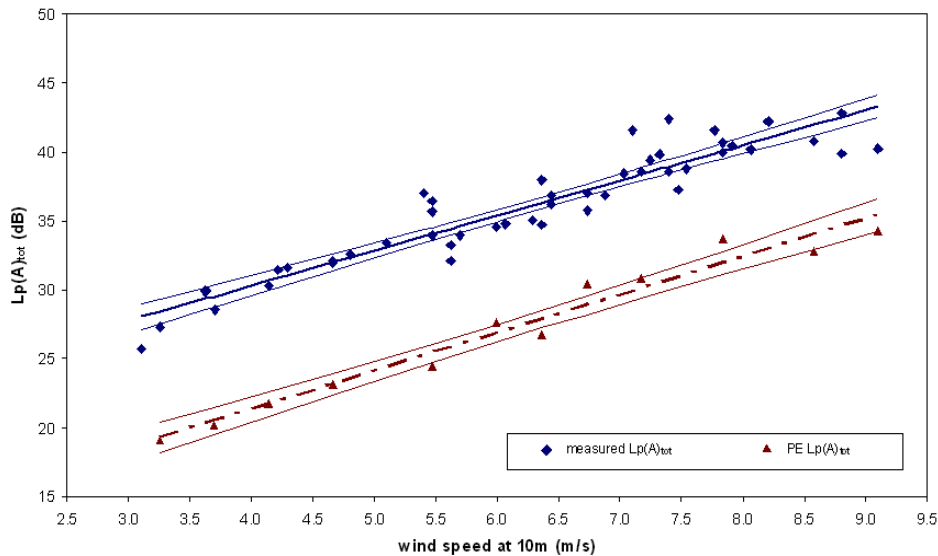


Figure 5.7: PE calculated total, A-weighted sound pressure levels compared to the measured total, A-weighted sound pressure levels. The best fit and confidence interval at 95% for both sets are also drawn.

As for the standard calculations, the PE calculations deviate significantly from the measured levels, for the measured wind speed range. The deviation of the PE model is about 8 dB, in the same order as for the standard calculations.

### **Influence of the meteorology**

In the process of modeling the outdoor sound propagation, the difference between the Swedish standard and the PE method is that the PE model takes into account the meteorological data. The wind speed is assumed to have the strongest influence on the sound propagation, and thereafter the temperature gradient and air absorption, the latter influenced mainly by air relative humidity and temperature. As the PE model does not perform better than the standard, it is thus interesting to study the influence of the meteorology on the sound propagation.

The measured total, A-weighted sound pressure levels increase with wind speed (see Section 5.2.1). This increase is supposedly caused by two phenomena:

- the increase of the source output sound power with wind speed (see Section 5.1.1): the stronger the wind, the stronger the noise source;
- the strengthening in sound speed profile with wind speed: this causes downward refraction and a focusing effect of the propagated sound at the receiver point.

If the source output sound power is artificially set to a constant reference level for all wind speeds, the PE predictions for the 12 selected measurements will only show the influence of the meteorology on the sound propagation.

Figure 5.8 shows the PE predictions for the 12 selected measurements, assuming a constant reference source output sound power, at a wind speed 3 m/s at 10 m.

The total, A-weighted sound pressure levels are spread over a range of 1.5 dB. No clear trend appears whereas an increasing trend with wind speed was expected. The small variations within the 1.5 dB range are due to the temperature gradient and the air absorption.

It can be concluded that in the case of this study, with this geometry (high noise source and relatively short propagation range) and assumed profiles (logarithmic profile for wind speed), the focusing effect of propagated sound, due to downward refraction, is not large enough to influence the immission levels at receiver point. The increase of the total, A-weighted sound pressure levels with wind speed is largely governed by the increase of the source output sound power.

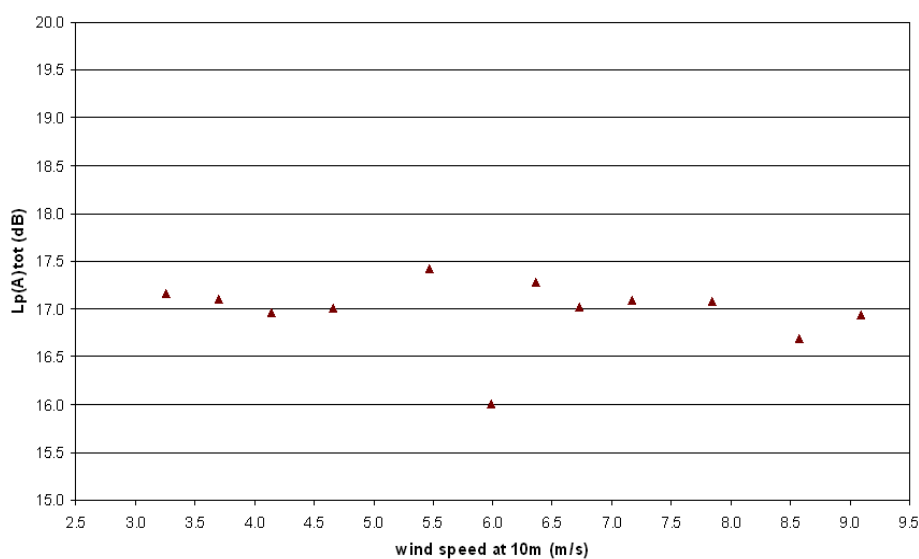


Figure 5.8: Influence of increasing wind speeds on calculated  $L_P(A)_{tot}$  for PE calculations.

### Alternative prediction models

The PE calculations are time consuming and it appears that there is no need of an advanced prediction technique for this case. Alternative prediction techniques, such as an analytical model or an engineering method may give equally valid results.

Analytical calculations are made corresponding to the 12 selected measurements, assuming no wind. Also, the freeware program WiTuProp is used as the engineering method. It is based on geometric ray-tracing, and assumes ground with finite impedance and a linear sound speed profile.

Figure 5.9 presents the comparison between the 4 tested prediction methods (Swedish standard, PE method, analytical method and WiTuProp), for the 12 selected measurements.

For each of the 12 tested cases, all the models agree well. Along the measured wind speed range, the predictions spread within a range of maximum 3 dB.

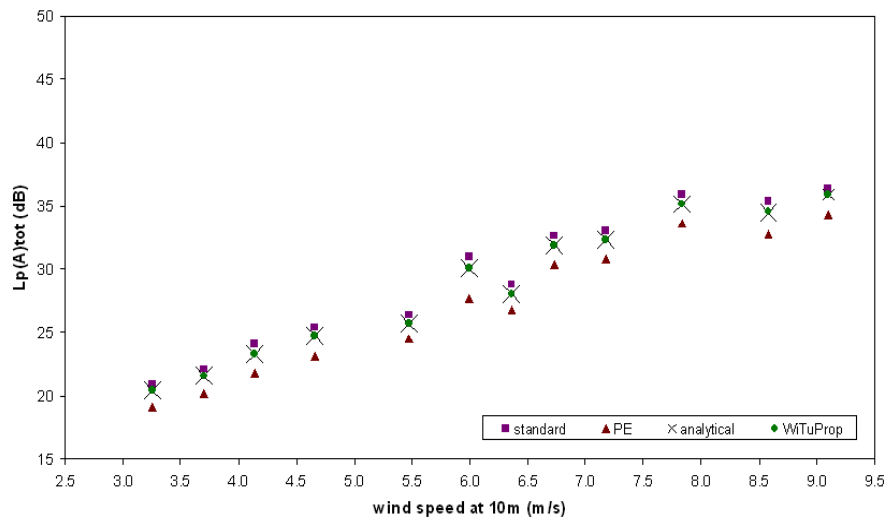


Figure 5.9: Comparison of calculated total, A-weighted sound pressure levels for the tested prediction methods, for the 12 selected measurements.

In Figure 5.10, the calculations of the 4 prediction methods are compared to the measured total, A-weighted sound pressure levels and are plotted as a function of wind speed at 10 m. A linear trend line is fitted for all set of data points,

$$\begin{aligned}
 \text{measured } L_P(A)_{tot} : & \quad L_P(A)_{tot} = 2.5u_{10} + 20.1 \\
 \text{standard } L_P(A)_{tot} : & \quad L_P(A)_{tot} = 3.0u_{10} + 11.4 \\
 \text{PE } L_P(A)_{tot} : & \quad L_P(A)_{tot} = 2.8u_{10} + 10.3 \\
 \text{analytical } L_P(A)_{tot} : & \quad L_P(A)_{tot} = 2.8u_{10} + 11.6 \\
 \text{WiTuProp } L_P(A)_{tot} : & \quad L_P(A)_{tot} = 2.8u_{10} + 11.6
 \end{aligned} \tag{5.9}$$

with correlation coefficients exceeding 0.89.

As stated above, the prediction methods agree fairly well. The models give similar predictions along the measured wind speed range.

The trend lines, drawn for each set of data points, describe the relationship between the wind speed at 10 m  $u_{10}$  and the measured total, A-weighted sound pressure levels  $L_P(A)_{tot}$  for the measurements and the models. These relationships consist of a  $u_{10}$ -coefficient (or slope), which depicts how much the sound pressure levels increase when the wind speed increases, and a constant coefficient, which sets a minimum level to the trend line.

The slopes of all trend lines are of the same order, from 2.5 to 3.0 dB/(m/s). This means that the prediction methods depict correctly the increase of the sound pressure levels with wind speed.

The deviation of the calculation results from the measurement results comes from

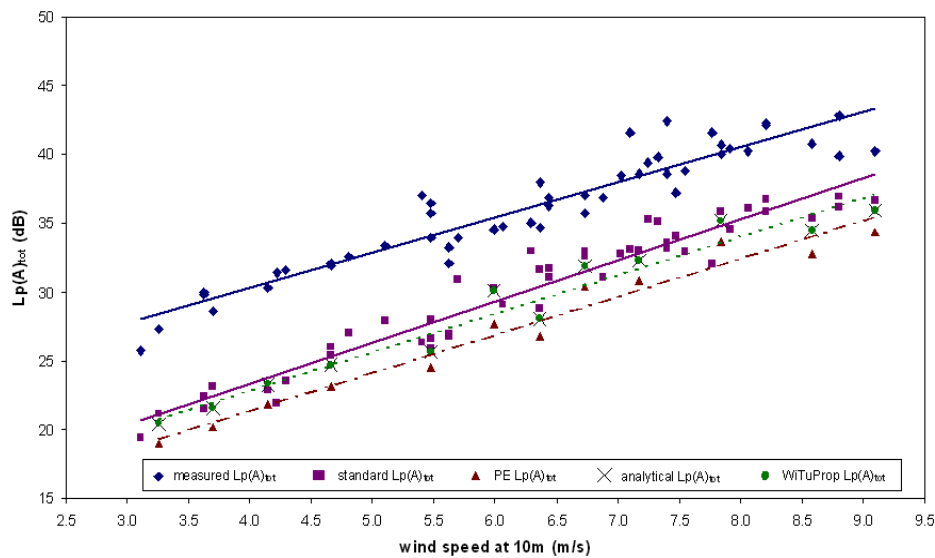


Figure 5.10: Calculated total, A-weighted sound pressure levels compared to the measured total, A-weighted sound pressure levels. The best fit for all sets of data points are displayed.

the difference in the constant coefficients which range from 10.3 to 20.1 dB. This corresponds to a bias error between measurements and calculations which reaches up to 9 dB.

Finally, the standard calculations attain the highest values amongst the models calculations. In this respect, the Swedish standard for wind turbine noise correspond to a worst case for calculating noise immission levels.

## 5.3 Discussion

### 5.3.1 Methodological considerations

At long distances (>300 m), the signal-to-noise ratio can be low, and noise immission measurements of a wind turbine can be influenced by background noise. In such cases, it is necessary to try to increase this ratio.

Mounting the microphone on a vertical reflecting board is a way of improving the signal-to-noise ratio:

- the picked-up signal is increased by 6 dB due to the reflection of the incident pressure on the rigid surface;
- the microphone is sheltered from other sources located behind the board.

In addition, wind-induced noise in the microphone is an important issue when measuring outdoors in strong wind conditions. Hence, it is vital to be aware of its

potential influence on the measurements and try to reduce this so-called pseudo-noise.

In Fégeant (1998), a study is conducted in order to determine the reduction of the wind-induced noise thanks to the use of a vertical reflecting board. The action of the board on the oncoming wind flow is called blocking effect which reduces the velocity as the stream approaches the board surface. On the side which faces the oncoming flow appears a stagnation point which characterizes a division of the stream and where the mean velocity is zero. Placing the microphone at the board center, i.e. at the stagnation point, ensures a very low pseudo-noise due to the zero mean velocity. The maximum effect is obtained when the board is orthogonal to the wind direction, and for increasing board sizes.

In Ljunggren (1997), an additional way of reducing the wind-induced noise is suggested. The use of an extra, large secondary windscreen together with the usual windscreen is beneficial. However, particular care is to be taken to rigidly attach the windscreen onto the board, as a slight gap between the windscreen and the board surface leads to a drastic increase of the wind noise.

In this study, both the above precautions were undertaken to reduce the wind-induced noise.

No emission measurements were carried out in this study even though the source output sound power is a crucial parameter for the prediction of the wind turbine noise. A key question is whether the sound power estimation (see Section 5.1.1) corresponds to the real emission levels, i.e. the subject wind turbine is not deviating from typical wind turbines of the same size and type.

In September 2005, emission measurements were conducted by Pontus Thorsson (Akustikverkstan i Skaraborg AB) on the same wind turbine, for a wind speed of 7.6m/s. Those measurements fitted well with the sound power estimation made according to Equation (5.1). The calculation made in this study overestimates the measured sound power by 0.5 dB. Furthermore, the source frequency spectrum for the  $\frac{1}{3}$ -octave bands 50-2500 Hz was retrieved from the same measurements. In van den Berg (2003), two frequency spectra for the octave bands 63-4000 Hz are given. The three spectra agreed well for all frequency bands.

### 5.3.2 Main findings

Very few studies have made these types of long term measurements. For the studies in van den Berg (2003) and Ljunggren (1997), such measurements were performed and led to precious suggestions concerning wind turbine noise assessment. In van den Berg (2003), valuable advice was given to estimate the source output power  $L_W(A)_{tot}$  from the blades' *rpm* rather than from the wind speed at 10 m. The recommendations in Ljunggren (1997) emphasized an improved measurement method for wind turbine noise. Solutions were investigated for improving the signal-to-noise ratio in immission measurements. Factors for uncertainty

in emission measurements were brought to light.

The results obtained in this study have shown that calculations made according to several prediction methods for wind turbine noise (Swedish standard, PE, analytical methods, and WiTuProp) deviate from measured sound immission levels for downwind propagation. It is important to note that all calculations were made using real measured meteorological data. In the same time, the tested models agreed within a range of 3 dB, and all accurately described the increase of sound pressure levels with increasing wind speed. The deviation of the calculations from the measurements comes from a bias error which reaches up to 9 dB. Among the prediction methods, the Swedish standard for wind turbine noise is the most conservative as it attained the highest predictions.

Several possible reasons arise to explain the deviations between measurements and calculations. First, there could be an insecurity of the output power level  $L_W(A)$  in the source model, which would cause the bias error in the calculation results. A too small constant term in Equation (5.1) would explain the low resulting levels of the model calculations. It appears that in wind turbine noise assessment, the source model stays a weak and difficult point.

Another reason could be that the measured immission levels are overestimated because of the influence of background noise or the influence of wind-induced noise. The level of wind-induced noise could not be quantitatively estimated. However, due to the measurement set-up and equipment (use of a hard board and a secondary windscreen), and to the fact that the signals have been listened through, the risk of contamination by wind-induced noise is strongly reduced.

The results show that the meteorology does not have a large influence on the sound propagation in this study. A wind profile according to a logarithmic or linear model gave negligible influence on the sound pressure levels, compared with a constant sound speed profile. However, at longer ranges or for a lower source height, larger effects can be expected. In addition, for more extreme sound speed profiles (for example, during night-time), it is expected that higher sound pressure levels can occur, for the same input data (geometry, ground properties, wind speed at 10 m, temperature gradient, relative humidity). In these circumstances, calculations based on the Nord2000 model (Kragh and Sondergaard 2005) (similar to WiTuProp) made for atmospheres with linear sound speed profiles, cannot be expected to give valid results. For such cases the PE would be useful.

# Chapter 6

## Conclusion

---

The conclusion recalls the thesis problematic, the implemented outdoor sound propagation models and the results given by the analysis of the measurements and the predictions of the models.

---

The number of wind turbines has been growing in Sweden, and the noise induced by their operation has become more problematic. The Swedish standard for wind turbine noise does not include variations of meteorological data in its outdoor sound propagation model and can therefore be questioned whether it satisfactory predicts wind turbine noise immission levels. The goal of the thesis was to compare the Swedish standard calculations to the measurements results; second, to determine if the designed PE model for outdoor sound propagation can give better prediction; finally, to determine how large the meteorological influence is on immission levels at receiver point and what the reasons are for possible deviations between measurements and calculations.

The outdoor sound propagation is a complex acoustic process. It includes several phenomena which must be understood in order to accurately calculate the propagation of sound outdoors. These phenomena are linked to different interpretation of the propagation medium. In first approximation, the atmosphere can be seen as a homogeneous medium. The propagated sound will be influenced by the spreading of the sound waves, by the atmospheric absorption and by the effects of the ground. To further represent the atmosphere, variations of temperature and wind speed over space is taken into account. This implies that atmospheric refraction is taken into account for the sound propagation.

Several prediction methods have been developed to solve the complex problems of outdoor sound propagation. Two of these methods were pointed out: the Fast Field Program (FFP) and the Parabolic Equation (PE) method. A PE model for outdoor sound propagation was implemented and validated. The validation consisted of comparison between PE calculations and analytical solution for a case where wind is neglected. A comparison was made with the FFP calculation for a case with wind influence.

Simultaneous measurements of acoustic data and meteorological variables were performed over a month in order to provide a realistic set of atmospheric conditions and sound pressure levels. Measurements were made on a flat land area, at a distance of 530 m from a wind turbine. In total, more than 700 measurements were

done within a range of wind speed from 0 to 18 m/s.

The proposed model for outdoor sound propagation based on the PE method was tested for calculating noise immission levels. The work was innovative in that the designed model considered the sensitivity of outdoor sound propagation to meteorological parameters, in the way that a logarithmic profile was considered. Other prediction methods were used to calculate the sound pressure levels: the Swedish standard for wind turbine noise prediction, the ray-based method WiTuProp, and an analytical solution.

The measurements were examined in terms of total, A-weighted sound pressure levels, and their dependence on the wind speed at 10 m height and on the temperature gradient. The results showed a relation between the measured sound pressure levels and the wind speed, due to the increased source strength with increased wind speed. The influence on sound propagation of the meteorology was studied and found to be negligible for the setting and assumed profiles.

Significant deviations were shown between the results from the measurements and those from calculations, using different prediction methods: the method according to the standard, the PE method, the ray-based method WiTuProp, and an analytical solution. The prediction methods all underestimated the measured results, by about 5 to 8 dB in A-weighted sound pressure levels. The prediction methods tried in this study agreed fairly well, within a 3 dB range.

As the final conclusion, a possible error of output sound power level,  $L_W(A)$ , in the source model is suggested as the main reason for the discrepancy between the measured and the calculated sound pressure levels.

# Appendix A

## Fast Field Program FFP

---

Two different numerical methods are used in this work to design a model for outdoor sound propagation. This appendix aims at presenting one of them, the Fast Field Program (FFP). The numerical scheme is described and the choices and the limitations concerning the implementation of the calculation model are summed up. The description follows the one given by Salomons (2001).

---

### A.1 Solution of the Helmholtz equation

Equation (2.2) is the basic equation of the FFP method. The axisymmetric assumption is used (i.e. rotational symmetry around the z-axis). Thereby the three-dimensional Helmholtz equation is simplified to a two-dimensional equation. In the horizontal wave number domain, for a monopole source of unit amplitude at position  $\vec{r}_s = (0, 0, z_s)$ , this equation becomes

$$k_{eff}^2 \frac{\partial}{\partial z} \left( \frac{1}{k_{eff}^2} \frac{\partial Q}{\partial z} \right) + k_z^2 Q = -\sqrt{2\pi k_r} \delta(z - z_s) \quad (\text{A.1})$$

where  $k_z^2 = k_{eff}^2 - k_r^2$ .  $Q$  represents the Fourier transform of the complex quantity  $q_c(\vec{r}) = \sqrt{r} \cdot p_c(\vec{r})$ . The wave number is  $k_{eff} = \frac{\omega}{c_{eff}}$  where  $c_{eff} = c + u$  is the effective sound speed;  $u$  is the wind velocity in the r-direction, from source to receiver.

The FFP principle is to assume a vertical profile of the wave number  $k_{eff}(z)$  in layers. The profile is approximated by dividing the atmosphere into horizontal layers for which  $k_{eff}$  is constant (see Figure A.1).

The heights of the interfaces between the layers are  $z_j$ ,  $j = 1, 2, \dots, N$  with  $z_1 = 0$  the ground surface height, and  $z_m = z_s$  the source height. As  $k_{eff}$  is constant within a layer, Equation (A.1) reduces to

$$\partial_z^2 Q + k_z^2 Q = -\sqrt{2\pi k_r} \delta(z - z_s), \quad \text{for } z_j \leq z < z_{j+1} \quad (\text{A.2})$$

In the equation above, the notations  $\partial_r$  and  $\partial_z$  are used for the derivatives  $\frac{\partial}{\partial r}$  and  $\frac{\partial}{\partial z}$ , respectively.

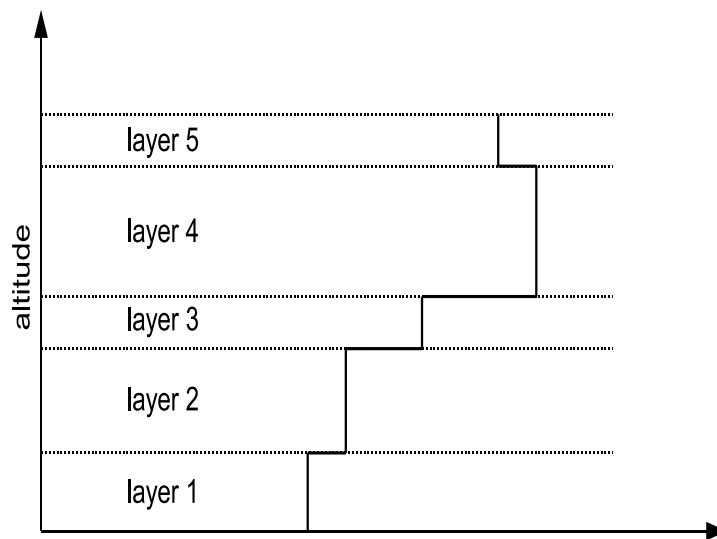


Figure A.1: In the FFP, the atmosphere is divided into layers. Within a layer, the wave number  $k(z)$  is constant.

This equation shows that rapid variations of the wave number with height require a large amount of thin layers. In layer  $j$ , the solution to Equation (A.2) is written as

$$Q_j = A_j e^{ik_{zj}z} + B_j e^{-ik_{zj}z} \quad \text{for } z_j \leq z \leq z_{j+1} \quad (\text{A.3})$$

where  $k_{zj}$  is the value of  $k_z$  in the layer and  $A_j$  and  $B_j$  are constants.

At the top of the physical domain, between  $z_{N-1}$  and  $z_N$ , only an upward traveling wave is present, which sets the boundary condition to  $B_{N-1} = 0$ <sup>1</sup>.

At the bottom of the physical domain, for  $z \leq 0$  the solution to Equation (A.2) is written as

$$Q_0 = B_0 e^{-ik_0 z} \quad (\text{A.4})$$

where  $B_0$  is a constant and  $k_0$  is the wave number in the ground.

The constants  $A_j$  and  $B_j$  are derived from the boundary conditions at the interfaces:

- the acoustic pressure is continuous at all interfaces,

$$Q_j(z_j) = Q_{j-1}(z_j), \quad \forall j \quad (\text{A.5})$$

<sup>1</sup>On a numerical point of view, this condition implies that this highest layer must be chosen above the region where sound is refracted downward to the receiver.

- the acoustic normal velocity is continuous at all interfaces, except at the source height,  $z = z_m$ . With the Fourier transform of the normal velocity given by  $W = \frac{1}{i\omega\rho} \frac{1}{\sqrt{r}} \cdot \partial_z Q$ ,

$$\frac{1}{i\omega\rho_j} \cdot \partial_z Q_j(z_j) = \frac{1}{i\omega\rho_{j-1}} \cdot \partial_z Q_{j-1}(z_j), \quad \forall j \neq m \quad (\text{A.6})$$

$$\partial_z Q_m(z_m) = \partial_z Q_{m-1}(z_m) - \sqrt{2\pi k_r}, \quad \text{for } j = m \quad (\text{A.7})$$

The boundary conditions for  $z_1 = 0$  give the relation

$$A_1 = \frac{k_{z1} - \frac{k(z_1)}{z_s}}{k_{z1} + \frac{k(z_1)}{z_s}} \cdot B_1 = R(k_{z1}) \cdot B_1 \quad (\text{A.8})$$

where  $Z_s$  is the normalized ground impedance and  $R(k_{z1})$  is the plane-wave reflection coefficient.

The other boundary conditions would help derive the formulation for the constants  $A_j$  and  $B_j$  in a set equation. However, another approach is preferred. From Equation (A.3) the following relations are derived

$$\begin{aligned} Q_j(z + \Delta z) &= \cos(k_{zj}\Delta z) Q_j(z) + \frac{1}{k_{zj}} \sin(k_{zj}\Delta z) \partial_z Q_j(z) \\ \partial_z Q_j(z + \Delta z) &= -k_{zj} \sin(k_{zj}\Delta z) Q_j(z) + \cos(k_{zj}\Delta z) \partial_z Q_j(z) \end{aligned} \quad (\text{A.9})$$

for  $z$  and  $z + \Delta z$  within a layer  $j$ . The quantities  $\cos(\omega)$  and  $\sin(\omega)$  are defined as

$$\begin{aligned} \cos(\omega) &= \frac{e^{i\omega} + e^{-i\omega}}{2} \\ \sin(\omega) &= \frac{e^{i\omega} - e^{-i\omega}}{2i} \end{aligned} \quad (\text{A.10})$$

The relations (A.9) are used to determine the quantities  $Q_j(z_j)$ .

## A.2 Extrapolation from the ground and the top to the source

The constants  $A_j$  and  $B_j$  are numerically found from an iterative approach using extrapolation. The extrapolation starts at height  $z_1 = 0$ . Arbitrarily,  $B_1$  is set to 1. From Equation (A.3) and Equation (A.8),

$$\begin{aligned} Q_1(z_1) &= R(k_{z1}) + 1 \\ \partial_z Q_1(z_1) &= ik_{z1} [R(k_{z1}) - 1] \end{aligned} \quad (\text{A.11})$$

The values of quantities  $Q_{j-1}(z_j)$  and  $\partial_z Q_{j-1}(z_j)$  are determined successively for  $j = 2, \dots, m$  by using Equation (A.11), Equation (A.9) with  $z = z_j$  and  $\Delta z = z_{j+1} - z_j$ , and Equation (A.5) and Equation (A.6). The final values  $Q_{m-1}(z_m)$  and  $\partial_z Q_{m-1}(z_m)$  at the source height  $z_m$  are denoted  $Q_{m,lower}$  and  $\partial_z Q_{m,lower}$ , respectively (lower region).

For the next step, the extrapolation starts at height  $z_N$ . Arbitrarily,  $Q_{N-1}(z_N)$  is set to 1. From Equation (A.3), with  $B_{N-1} = 0$ ,

$$\begin{aligned} Q_{N-1}(z_N) &= 1 \\ \partial_z Q_{N-1}(z_N) &= ik_{zN} \end{aligned} \quad (\text{A.12})$$

The values of quantities  $Q_j(z_j)$  and  $\partial_z Q_j(z_j)$  are determined successively for  $j = N-1, N-2, \dots, m$  by using Equation (A.12), Equation (A.9) with  $z = z_{j+1}$  and  $\Delta z = z_j - z_{j+1}$ , and Equation (A.5) and Equation (A.6). The final values  $Q_m(z_m)$  and  $\partial_z Q_m(z_m)$  at the source height  $z_m$  are denoted  $Q_{m,upper}$  and  $\partial_z Q_{m,upper}$ , respectively (upper region).

### Field at receiver

As  $B_1 = 1$  and  $Q_{N-1} = 1(z_N)$  were arbitrarily set, only the ratios  $\frac{\partial_z Q_j}{Q_j}$  are correct. The boundary condition at the source height  $z_m$  gives

$$\frac{\partial_z Q_{m,upper}}{Q_{m,upper}} Q_m - \frac{Q_{m,lower}}{\partial_z Q_{m,lower}} Q_m = -\sqrt{2\pi k_r} \quad (\text{A.13})$$

where  $Q_m$  is the correct value of  $Q$  at  $z_m$ . Hence,

$$Q_m = \frac{-\sqrt{2\pi k_r}}{\frac{\partial_z Q_{m,upper}}{Q_{m,upper}} - \frac{Q_{m,lower}}{\partial_z Q_{m,lower}}} \quad (\text{A.14})$$

Now the values  $Q_j$  can be scaled to the correct values, by multiplication by the factor

$$\begin{aligned} \frac{Q_m}{Q_{m,upper}}, & \quad \text{for } z_j > z_m \\ \frac{Q_m}{Q_{m,lower}}, & \quad \text{for } z_j < z_m \end{aligned} \quad (\text{A.15})$$

Finally, an inverse Fourier transform of the quantities  $Q_j$  yields the complex pressure amplitude in the spacial domain.

$$q_c(r, z) = \sqrt{r} p_c(r, z) = \frac{1}{\pi\sqrt{2}} \int_{-\infty}^{+\infty} \left( e^{ik_r r} + e^{-ik_r r} \right) Q(k_r, z) dk_r \quad (\text{A.16})$$

### A.3 Deformation of the integration path

The integrand in Equation (A.16) has poles on the integration path at  $k_r = k$  and  $k_r = -k$ . To avoid the poles, the integration is made along the deformed integration path shown on Figure A.2.

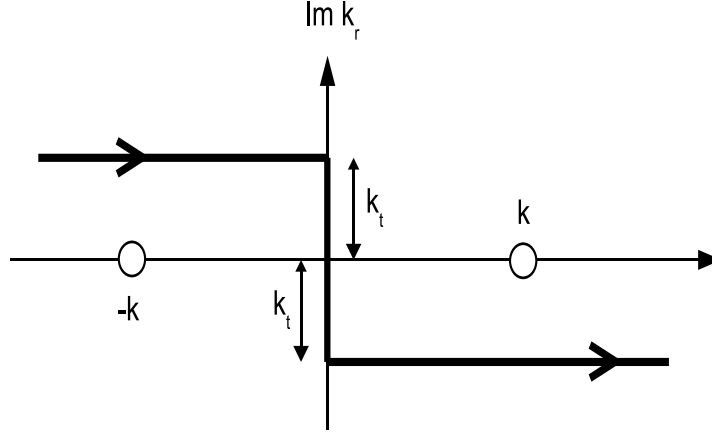


Figure A.2: The deformed integration path avoids the poles  $k_r = \pm k$  on the real axis

For positive  $k_r$ , a small imaginary term  $-ik_t$  is added, and for negative  $k_r$ , the opposite imaginary term  $ik_t$  is added, where  $k_t$  is a small positive number. The integral in Equation (A.16) can be transformed to an integral over positive wave numbers  $k_r$  only, using the relation  $Q(-k_r, z) = -iQ(k_r, z)$ . Therefore, Equation (A.16) becomes

$$q_c(r, z) = \sqrt{r} p_c(r, z) = \frac{1-i}{\pi\sqrt{2}} \int_0^{+\infty} \left( e^{ik_r r} + e^{-ik_r r} \right) Q(k_r, z) dk_r \quad (\text{A.17})$$

For the numerical evaluation of this integral, the variable  $k_r$  is discretized as

$$k_{r,n} = k_{s,n} - ik_t \quad (n = 1, 2, \dots, M) \quad (\text{A.18})$$

with

$$k_{s,n} = \frac{1}{2}\Delta k, \frac{3}{2}\Delta k, \dots, k_{s,M} \quad (\text{A.19})$$

$\Delta k$  is the wave number spacing. The solution  $q_c$  given by Equation (A.17) is periodic in  $r$  by the discretization, with periodic distance  $\frac{2\pi}{\Delta k}$ . The wave number spacing  $\Delta k$  should be chosen small enough to ensure that this periodicity does not affect the field  $q_c$  at the receiver: one can use, for example,  $\frac{2\pi}{\Delta k} \geq 3r$ .

The choice of the maximum wave number  $k_{s,M}$  depends on the frequency. A good value is  $k_{s,M} \approx \frac{3\omega}{c(z_1=0)}$ . For the small positive number  $k_t$  one can use the value  $\Delta k$ .

The truncation of the integration interval in Equation (A.17) at the maximum wave number  $k_{s,M}$  produces small rapid numerical oscillations of  $q_c$  as a function of  $r$ . This phenomenon is eliminated with a Hanning window function as a factor in Equation (A.17) (the Hanning window is unity, and goes smoothly to zero near the integration limit).

# Appendix B

## Parabolic Equation (PE) method

---

This appendix presents the other numerical method which is used in the thesis in order to design a model for outdoor sound propagation: the Parabolic Equation method (PE method). The numerical scheme is described and the choices and the limitations concerning the implementation of the calculation model are summed up. The PE method is rather a family of method: the one described in the following is the Crank-Nicholson PE method. The description mainly follows the one given by Salomons (2001).

---

### B.1 Crank-Nicholson PE

The Crank-Nicholson PE method is based on the axisymmetric approximation (i.e. rotational symmetry around the z-axis is assumed). Thus, only a plane in the r,z-domain is studied.

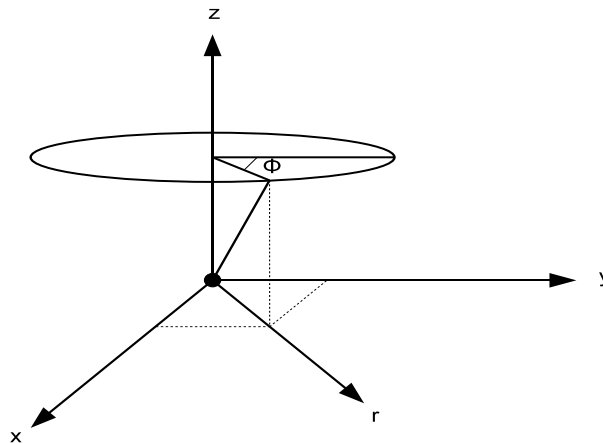


Figure B.1: Rectangular  $xyz$  coordinates and cylindrical  $rz\phi$  coordinates

Starting from the Helmholtz wave equation, the parabolic wave equation used in the CNPE is retrieved. The Helmholtz wave equation, in a medium where axisymmetry is assumed, takes the form

$$\frac{1}{r} \frac{\partial}{\partial r} \left( r \frac{\partial p_c}{\partial r} \right) + \frac{\partial^2 p_c}{\partial z^2} + k_{eff}^2 p_c = 0 \quad (\text{B.1})$$

where the cylindrical coordinates (see Figure B.1) are used.  $p_c$  is the complex sound pressure and  $k_{eff} = \frac{\omega}{c_{eff}}$  is the wave number, where  $\omega$  is the angular frequency and  $c_{eff}$  is the effective sound speed. Later the subscripts 'eff' and 'c' will be omitted, so  $k_{eff} \equiv k$ ,  $c_{eff} \equiv c$  and  $q_c \equiv q$ .

The quantity  $q_c$  is defined

$$q_c = p_c \sqrt{r}, \quad \forall r \neq 0 \quad (\text{B.2})$$

and introduced in Equation (B.1), gives

$$\frac{\partial^2 q_c}{\partial r^2} + \frac{1}{4r^2} q_c + \frac{\partial^2 q_c}{\partial z^2} + k^2 q_c = 0 \quad (\text{B.3})$$

The far-field approximation is applied (i.e.  $r \cdot k \gg 1$ ) so the second term on the left-hand side can be neglected, leading to

$$\frac{\partial^2 q_c}{\partial r^2} + \frac{\partial^2 q_c}{\partial z^2} + k^2 q_c = 0 \quad (\text{B.4})$$

In the CNPE method, the field  $q(r, z)$  is computed on a grid in the  $r, z$ -plane (see Figure B.2). The computation starts at  $r = 0$  with a starting function  $q(0, z)$ . This function is extrapolated step-wise in the positive  $r$ -direction, from range  $r$  to range  $r + \Delta r$ . This process yields the complete field  $q(r, z)$ . Accurate results are obtained if the horizontal grid spacing  $\Delta r$  and the vertical grid spacing  $\Delta z$  do not exceed about  $\frac{\lambda}{10}$ , where  $\lambda$  is the wavelength  $\frac{c}{f}$ .

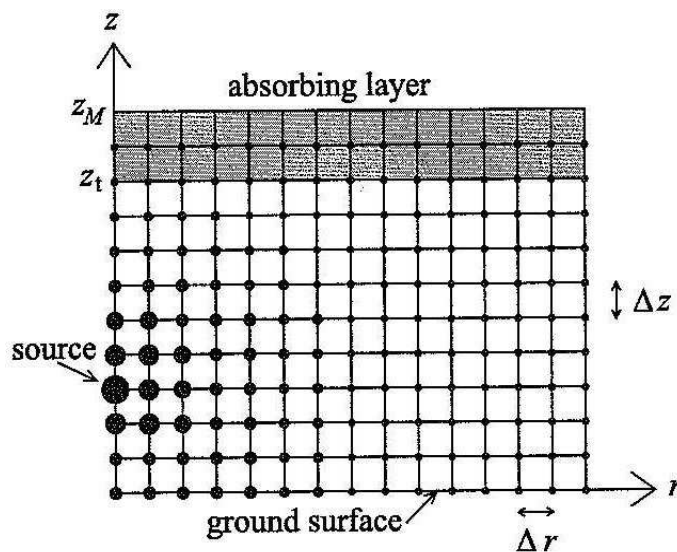


Figure B.2: The PE computational grid

The grid has a finite height. To eliminate reflections from the top of the grid, an artificial absorbing layer is used above the height  $z_t$ . The ground boundary condition

is taken into account with the complex ground impedance. Within an extrapolation step, the wave number  $k$  is a function of  $z$  only.

The original formulation of the CNPE is limited to quite small elevation angles. An alternate wide-angle formulation allows angles up to  $35^\circ$ .

## B.2 Narrow-angle CNPE

The solution of Equation (B.4) can be written as

$$q(r, z) = \psi(r, z)e^{ik_0r} \quad (\text{B.5})$$

where  $k_0$  is the value of the wave number at the ground surface. The factor  $e^{ik_0r}$  represents a plane wave traveling in the positive  $r$ -direction, and oscillates rapidly with  $r$ . The function  $\psi(r, z)$  is the carrier and varies slowly with  $r$ . Substitution of Equation (B.5) into Equation (B.4) gives

$$\partial_r^2 \psi + 2ik_0 \partial_r \psi + \partial_z^2 \psi + (k^2 - k_0^2) \psi = 0 \quad (\text{B.6})$$

where the notation  $\partial_r \equiv \frac{\partial}{\partial r}$  and  $\partial_z \equiv \frac{\partial}{\partial z}$  are used.

Defining the two operators  $P$  and  $Q$  as,

$$P = \partial_r \quad , \quad Q = \sqrt{\frac{c_0^2}{c^2} + \frac{1}{k_0^2}} \cdot \partial_z^2 \quad (\text{B.7})$$

it is possible to rewrite Equation (B.6) as

$$(P^2 + 2ik_0P + k_0^2(Q^2 - 1)) \psi = 0 \quad (\text{B.8})$$

Equation (B.8) can be separated into components,

$$[P + ik_0 - ik_0Q] \cdot [P + ik_0 + ik_0Q] \psi - ik_0 [PQ - QP] \psi = 0 \quad (\text{B.9})$$

The first bracket represents an outgoing wave, the second the incoming wave, and  $[PQ - QP]$  is the commutator of the operators  $P$  and  $Q$  which is 0 when the speed of sound and the wave number are only height dependent,  $c = c(z)$  and  $k = k(z)$ .

Including the approximation of a one-way wave equation and considering only the outgoing wave, Equation (B.9) becomes

$$\begin{aligned}
 [P + ik_0 - ik_0Q] \psi = 0 & \Leftrightarrow P\psi = ik_0 [Q - 1] \psi \\
 \Rightarrow \partial_r \psi = ik_0 \left[ \sqrt{\frac{c_0^2}{c^2} + \frac{1}{k_0^2} \cdot \partial_z^2} - 1 \right] \psi & \quad (B.10)
 \end{aligned}$$

Before Equation (B.10) is implemented, it is important to evaluate the assumptions that lead to the transformation of the initial Helmholtz equation into Equation (B.10), and how they could limit the applicability of the PE method. The first approximation is the far-field approximation necessary to write Equation (B.4), as the complex pressure amplitude  $p(r, z)$  is expressed as  $\frac{1}{\sqrt{r}} \cdot q(r, z)$ . When the PE method is applied to long distance outdoor sound propagation, a far field solution is acceptable, so this does not limit the solution. The second approximation is to neglect the commutator  $[PQ - QP]$  in Equation (B.9). In the case of both range and height dependence of the sound speed  $c$ , this approximation proved to lead to an error on second order in  $\Delta r$  (Arranz 1996). In the case of range independent media the commutator is exactly 0 and this leads to no error. The third approximation is to only consider the outgoing wave, thus no backscattered waves can be included in the calculations. Again, only far field solutions at relatively low height are wanted in this study, so this assumption will not limit the calculations.

The operator  $Q$  can be written as the squared-root function,

$$Q = \sqrt{1 + q} \quad , \quad q = \left( \frac{c_0^2}{c^2} + \frac{1}{k_0^2} \cdot \partial_z^2 \right) - 1 \quad (B.11)$$

Equation (B.10) can be solved as soon as the pseudo-differential operator  $Q$  is known. Several models exist: Tappert, Claerbout Padé (order 1), Greene, Padé (order 2). They develop  $\sqrt{1 + q}$  into different partial differential operators (see Table B.1).

Table B.1: *Different developments of the operator  $Q$*

Model	Formulation
Tappert	$\sqrt{1 + q} \approx 1 + \frac{1}{2}q$
Claerbout Padé (1)	$\sqrt{1 + q} \approx \frac{1+0,75q}{1+0,25q}$
Greene	$\sqrt{1 + q} \approx \frac{0,99987+0,79624q}{1+0,30102q}$
Padé (2)	$\sqrt{1 + q} \approx 1 + \frac{0,1382q}{1+0,06541q} + \frac{0,36180}{1+0,09549q}$

The narrow-angle formulation assumes the Tappert transformation. Thus Equation (B.10) becomes

$$Q = \sqrt{1 + q} \approx 1 + \frac{1}{2}q$$

$$\begin{aligned} \Rightarrow \partial_r \psi &= ik_0 [Q - 1] \psi \approx ik_0 \left[ 1 + \frac{1}{2}q - 1 \right] \psi \\ \Leftrightarrow \partial_r \psi &= \frac{1}{2} ik_0 q \psi \end{aligned} \quad (\text{B.12})$$

The last equation is called the narrow-angle parabolic equation.

### B.3 Wide-angle CNPE

The Tappert approximation for the square-root operator is accurate only for propagation at small elevation angle, up to about  $10^\circ$ . A more accurate expansion is the Claerbout Padé expansion

$$\sqrt{1+q} \approx \frac{1+0,75q}{1+0,25q} \quad (\text{B.13})$$

With Equation (B.13), the one-way wave equation Equation (B.10) becomes the wide-angle parabolic equation:

$$\left( 1 + \frac{1}{4} \right) \partial_r \psi = \frac{1}{2} ik_0 q \psi \quad (\text{B.14})$$

### B.4 Finite-difference solution of the CNPE

The narrow-angle and wide-angle parabolic equation derived in the two previous sections can be solved numerically by approximating the derivatives with finite differences.

In the case of the narrow-angle formulation, Equation (B.12) is rewritten as

$$\partial_r \psi = \alpha \partial_z^2 \psi + \beta \psi \quad (\text{B.15})$$

with  $\alpha = \frac{1}{2} \frac{i}{k_0}$  and  $\beta = \frac{1}{2} i \frac{k^2 - k_0^2}{k_0}$ . The grid shown in Figure B.2 is used, with grid points at heights

$$z_j = j \cdot \Delta z \quad \text{with } j = 1, 2, \dots, M. \quad (\text{B.16})$$

The field  $\psi$  at range  $r$  is denoted as a vector  $\vec{\psi}(r)$  with elements  $\psi_j = \psi(r, z_j)$ . Using the central difference formula

$$\left( \partial_z^2 \vec{\psi} \right)_{z_j} = \frac{\psi_{j+1} - 2\psi_j + \psi_{j-1}}{(\Delta z)^2}, \quad (\text{B.17})$$

Equation (B.15) is written as

$$\begin{aligned}
 \partial_r \begin{pmatrix} \psi_1 \\ \psi_2 \\ \dots \\ \psi_{M-1} \\ \psi_M \end{pmatrix} = & \\
 \left[ \begin{pmatrix} -2 & 1 & & & \\ 1 & -2 & 1 & & \\ & \dots & \dots & \dots & \\ & & 1 & -2 & 1 \\ & & & 1 & -2 \end{pmatrix} + \begin{pmatrix} \beta_1 & & & & \\ & \beta_2 & & & \\ & & \dots & & \\ & & & \beta_{M-1} & \\ & & & & \beta_M \end{pmatrix} \right] \begin{pmatrix} \psi_1 \\ \psi_2 \\ \dots \\ \psi_{M-1} \\ \psi_M \end{pmatrix} & \\
 + \gamma \begin{pmatrix} \psi_0 \\ 0 \\ \dots \\ 0 \\ \psi_{M+1} \end{pmatrix} &
 \end{aligned} \tag{B.18}$$

with  $\gamma = \frac{\alpha}{(\Delta z)^2}$  and  $\beta_j = \beta(z_j)$ .

The vector equation Equation (B.18) represents a set of  $M$  equations. Each equation relates an element  $\partial_r \psi_j$  to the element  $\psi_{j+1}$ ,  $\psi_j$ , and  $\psi_{j-1}$ . The last term on the on the right-hand side of Equation (B.18) contains the field  $\psi_0$  at the ground level  $z_0 = 0$  and the field  $\psi_{M+1}$  at height  $z_{M+1} = (M + 1)\Delta z$ . The field  $\psi_0$  at ground level is expressed as

$$\psi_0 = \sigma_1 \psi_1 + \sigma_2 \psi_2 \tag{B.19}$$

where coefficients  $\sigma_1$  and  $\sigma_2$  depend on the ground impedance. The field  $\psi_{M+1}$  is expressed as

$$\psi_{M+1} = \tau_1 \psi_M + \tau_2 \psi_{M-1} \tag{B.20}$$

where coefficients  $\tau_1$  and  $\tau_2$  are determined by the upper boundary condition.

Using Equation (B.19) and Equation (B.20), Equation (B.18) is simplified to the vector equation

$$\partial_r \vec{\psi} = (\gamma \cdot T + D) \vec{\psi} \tag{B.21}$$

where  $T$  is a tridiagonal matrix given by

$$T = \begin{pmatrix} -2 + \sigma_1 & 1 + \sigma_2 & & & & \\ & 1 & -2 & 1 & & \\ & & \dots & \dots & \dots & \\ & & & 1 & -2 & 1 \\ & & & & 1 + \tau_2 & -2 + \tau_1 \end{pmatrix} \quad (\text{B.22})$$

and  $D$  is a diagonal matrix given by

$$D = \begin{pmatrix} \beta_1 & & & & & \\ & \beta_2 & & & & \\ & & \dots & & & \\ & & & \beta_{M-1} & & \\ & & & & \beta_M & \end{pmatrix} \quad (\text{B.23})$$

Integration of Equation (B.21) from range  $r$  to range  $r + \Delta r$  gives

$$\int_r^{r+\Delta r} \partial_r \vec{\psi}(r) dr = (\gamma T + D) \int_r^{r+\Delta r} \vec{\psi}(r) dr \quad (\text{B.24})$$

$$\Rightarrow \vec{\psi}(r + \Delta r) - \vec{\psi}(r) = (\gamma T + D) \cdot \frac{\vec{\psi}(r + \Delta r) + \vec{\psi}(r)}{2} \times \Delta r \quad (\text{B.25})$$

$$\Rightarrow M_2 \vec{\psi}(r + \Delta r) = M_1 \vec{\psi}(r) \quad \text{where} \quad \begin{aligned} M_1 &= 1 + \frac{1}{2} \Delta r (\gamma T + D) \\ M_2 &= 1 - \frac{1}{2} \Delta r (\gamma T + D) \end{aligned} \quad (\text{B.26})$$

A PE step  $\vec{\psi}(r) \rightarrow \vec{\psi}(r + \Delta r)$  is reduced to the solution of Equation (B.26), which is a set of  $M$  linear equation for  $M$  unknowns  $\psi_j(r + \Delta r)$ . As  $M_1$  and  $M_2$  are tridiagonal matrices, the solution can be performed efficiently by Gauss elimination.

The passing from Equation (B.24) to Equation (B.25) includes the approximation of the term  $\int_r^{r+\Delta r} \vec{\psi}(r) dr$  by the term  $\frac{1}{2} [\vec{\psi}(r + \Delta r) + \vec{\psi}(r)] \Delta r$ . This approximation is called the Crank-Nicholson approximation.

In the case of the wide-angle formulation, the parabolic equation (B.14) differs from the narrow-angle parabolic equation (B.12) by the factor  $(1 + \frac{1}{4}q)$  on the left-hand side. Consequently, this factor yields a factor  $(1 + \frac{\gamma T + D}{2ik_0})$  on the left-hand side of Equation (B.21). This leads to the matrix Equation (B.26) with modified matrices  $M_1$  and  $M_2$  given by

$$\begin{aligned} M_1 &= 1 + \frac{1}{2} \Delta r (\gamma T + D) + \frac{\gamma T + D}{2ik_0} \\ M_2 &= 1 - \frac{1}{2} \Delta r (\gamma T + D) + \frac{\gamma T + D}{2ik_0} \end{aligned} \quad (\text{B.27})$$

The PE method based on Equation (B.26) and Equation (B.27) is called the Crank-Nicholson PE (CNPE) method.

## B.5 Boundary condition at the ground surface

At the ground surface, the boundary condition is

$$Z\rho c_0 = \left( \frac{p_c}{v_{c,n}} \right)_{z=0} \quad (\text{B.28})$$

where  $Z$  is the normalized ground impedance of the locally reacting ground surface,  $\rho c_0$  is the impedance of air just above the ground,  $p_c$  is the complex pressure amplitude, and  $v_{c,n}$  is the normal component of the complex air velocity amplitude.

The equations of acoustics give  $v_{c,n} = -\frac{1}{i\omega\rho}\partial_z p_c$ . Consequently, Equation (B.2) and Equation (B.5) give  $p_c = \frac{1}{\sqrt{r}}\psi(r, z)e^{ik_0 r}$  and,  $v_{c,n} = -\frac{1}{i\omega\rho}\frac{1}{\sqrt{r}}\partial_z\psi(r, z)e^{ik_0 r}$

Substitution in Equation (B.28) leads to

$$\begin{aligned} \left( \frac{\psi(r, z)}{-\frac{1}{i\omega\rho}\partial_z\psi(r, z)} \right)_{z=0} &= Z\rho c_0 \\ \Rightarrow \psi &= -Zc_0 \cdot \frac{1}{i\omega}\partial_z\psi_{z=0} \\ \Rightarrow \psi &= -Z \cdot \frac{1}{ik_0}\partial_z\psi_{z=0} \\ \Rightarrow \partial_z\psi_{z=0} + \frac{ik_0}{Z}\psi_{z=0} &= 0 \end{aligned} \quad (\text{B.29})$$

The second-order finite-difference approximation is used to express the derivative of  $\partial_z\psi$  (preferable for the wide-angle formulation)

$$\partial_z\psi_{z=0} = \frac{\psi_1 - \psi_0}{\Delta z} - \frac{1}{2}\Delta z \frac{\psi_2 - 2\psi_1 + \psi_0}{\Delta z^2} = \frac{-\frac{3}{2}\psi_0 + 2\psi_1 - \frac{1}{2}\psi_2}{\Delta z} \quad (\text{B.30})$$

Substitution in Equation (B.29) gives the following relation between  $\psi_0$ ,  $\psi_1$  and  $\psi_2$

$$\psi_0 = \frac{1}{3 - \frac{2ik_0\Delta z}{Z}} (4\psi_1 - \psi_2) \quad (\text{B.31})$$

The coefficients  $\sigma_1$  and  $\sigma_2$  in Equation (B.19) follow from this relation.

## B.6 Upper boundary condition

At the top surface, for  $z = z_M$ , a similar boundary condition as at the ground surface is used. The air normalized impedance  $Z = 1$  is used for the top surface normalized impedance. Following the same reasoning as for Equation (B.31) gives

$$\psi_{M+1} = \frac{1}{3 + 2ik_0\Delta z} (4\psi_M - \psi_{M-1}) \quad (\text{B.32})$$

The coefficients  $\tau_1$  and  $\tau_2$  in Equation (B.20) follow from this relation.

The numerical grid is truncated at height  $z = z_M$ . This can cause sound waves traveling upwards, to be reflected back into the region  $z < z_M$ . An absorbing layer just below the top surface, between  $z = z_t$  and  $z = z_M$  (see Figure B.2), can eliminate these reflections.

For this purpose, an imaginary term is added to the wave number  $k(z)$  for  $z_t < z < z_M$ . Sounds are gradually attenuated in the absorbing layer. Salomons (2001) gives a formulation for the imaginary term and writes the wave number as

$$k(z_t < z < z_M) = k(z) + iA_t \frac{(z - z_t)^2}{(z_M - z_t)^2} \quad (\text{B.33})$$

where  $A_t$  is a frequency dependent variable. Values for  $A_t$  are 1, 0.5, 0.4, 0.2 at the frequencies 1000, 500, 125, 30 Hz, respectively. For intermediate frequencies, linear interpolation can be used. A safe value for the thickness  $z_M - z_t$  of the absorbing layer is 50 wavelengths.

In order for the sound field not to be influenced by the absorbing layer, the height of the physical domain  $z_t$  should be chosen high enough. The value  $z_t$  is determined by the sound speed profile (downward refracting atmosphere) or the ground impedance (upward refracting atmosphere).

In the case of a downward refracting atmosphere, all curved sound waves from the source to the receiver should have their maximum heights below the absorbing layer. In this case, a minimum value for  $z_t$  can be  $z_t \geq \frac{r}{2\pi \frac{c_0}{b}}$ , with  $r$  the distance to the source, and  $b$  the logarithmic wind profile parameter. In the case of an upward refracting atmosphere, this limit is estimated as  $z_t \geq \lambda \frac{a^2 + b^2}{b^2}$ , where  $\lambda$  is the wavelength and  $a$  is the real part,  $b$  the imaginary part of the ground impedance (Arranz 1996).

## B.7 Starting field

The numerical solution for the narrow-angle or wide-angle parabolic equation has been reduced to the repeated solution of the tridiagonal matrix equation (B.26) for

a PE step  $\vec{\psi}(r) \rightarrow \vec{\psi}(r + \Delta r)$ . The computation starts at the source at  $r = 0$ , where a starting field  $\vec{\psi}(0, z)$  is required. The starting field represents a monopole source.

The starters are based on Gaussian distributions of the field at the initial position  $r_0$ . They are designed to closely match the far field pattern generated by a point source in a homogeneous medium. A first starter presented in literature (Galindo (1996)) is the Gaussian source

$$\psi(0, z) = \sqrt{k_0} \cdot e^{-\frac{k_0^2}{2}(z-z_s)^2} \quad (\text{B.34})$$

where  $z_s$  is the source height. The Gaussian source is the starter used for narrow-angle parabolic calculation. Several improvements have been made to solve the angular limitation. However, none of the starters include the ground properties, which leads to wrong predictions (Galindo (1996)) gets an extra attenuation of 5 dB in the prediction of sound pressure level relative to free field, in the case of a source located close to the ground).

Hence, to overcome this problem, the amplitude of the Gaussian source is modulated with the plane wave reflection coefficient for vertical incidence on the ground,

$$\psi(0, z) = \sqrt{\frac{k_0}{2}} \left[ e^{-\frac{k_0^2}{4}(z-z_s)^2} + \frac{Z-1}{Z+1} e^{-\frac{k_0^2}{4}(z+z_s)^2} \right] \quad (\text{B.35})$$

# Appendix C

## Statistical analysis

---

This appendix presents the statistical treatment which is applied to the data in the thesis. Regression analysis is illustrated with the calculation of the linear regression line and confidence intervals. The description mainly follows the one given by Altman (1991).

---

### C.1 Regression line

The equation of the least squares linear regression is  $Y = a + bX$  and estimates of  $a$  and  $b$  can be obtained easily. Denoting the observed data as  $x_i$  and  $y_i$  ( $i = 1, \dots, n$ ) it can be shown that the regression line must pass through the mean of the data  $(\bar{x}, \bar{y})$ . The estimated slope is given by

$$b = \frac{\sum (x_i - \bar{x})(y_i - \bar{y})}{\sum (x_i - \bar{x})^2}. \quad (\text{C.1})$$

The calculations can be simplified with the auto-correlation and cross-correlation for the values  $X$  and  $Y$ :

$$\begin{aligned} S_{xx} &= \sum x_i^2 - \frac{(\sum x_i)^2}{n} \\ S_{yy} &= \sum y_i^2 - \frac{(\sum y_i)^2}{n} \\ S_{xy} &= \sum x_i y_i - \frac{\sum x_i \sum y_i}{n}. \end{aligned} \quad (\text{C.2})$$

An easier way of calculating  $b$  is as

$$b = \frac{S_{xy}}{S_{xx}}. \quad (\text{C.3})$$

As the regression line passes through the mean  $(\bar{x}, \bar{y})$ , an estimate of  $a$  is simply

$$a = \bar{y} - b\bar{x}. \quad (\text{C.4})$$

So for any value  $x_0$  of  $X$ , the fitted value of  $Y$  predicted by the equation is

$$\begin{aligned} y_{fit} &= a + bx_0 \\ &= (\bar{y} - b\bar{x}) + bx_0 \\ &= \bar{y} + b(x_0 - \bar{x}) \end{aligned} \tag{C.5}$$

## C.2 Residual variation

The difference between an observed value  $y_0$  and fitted value  $y_{fit}$  is thus

$$y_0 - y_{fit} = y_0 - [\bar{y} + b(x_0 - \bar{x})], \tag{C.6}$$

and the value  $y_0 - y_{fit}$  is the residual for that individual. It is the sum of the squares of the residuals,  $\sum (y_i - y_{fit})^2$ , that is minimized by the least squares regression line, but their variance is of more interested:

$$s_{res}^2 = \frac{\sum (y_i - y_{fit})^2}{n - 2} \tag{C.7}$$

or for calculation

$$\begin{aligned} s_{res}^2 &= \frac{1}{n - 2} \left[ \sum y_i^2 - \frac{(\sum y_i)^2}{n} - b \left( \sum x_i y_i - \frac{\sum x_i \sum y_i}{n} \right) \right] \\ &= \frac{1}{n - 2} (S_{yy} - bS_{xy}). \end{aligned} \tag{C.8}$$

The square root of this expression, the residual standard deviation,  $s_{res}$ , is used in subsequent calculations.

## C.3 Confidence intervals

### C.3.1 Slope

The standard error of the slope,  $b$ , is strongly related to the residual standard deviation, being

$$se(b) = \frac{s_{res}}{\sqrt{S_{xx}}} \tag{C.9}$$

so that a 95% confidence interval for  $b$  is

$$b \pm t_{1-\frac{\alpha}{2}} \cdot se(b), \alpha = 0.05 \quad (\text{C.10})$$

where  $t_{1-\frac{\alpha}{2}}$  is the  $t$  distribution on  $n - 2$  degrees of freedom, with the probability  $\alpha$ . The slope is usually the aspect of most interest.

### C.3.2 Estimated $Y$ for a given $X$

The standard error of the estimate  $y_{fit}$  for a given value of  $X$ , say  $x_0$ , is given by

$$se(y_{fit}) = s_{res} \sqrt{\frac{1}{n} + \frac{(x_0 - \bar{x})^2}{S_{xx}}} \quad (\text{C.11})$$

and a 95% confidence interval is given by

$$y_{fit} \pm t_{0.975} \cdot se(y_{fit}) \quad (\text{C.12})$$

where  $t$  is on  $n - 2$  degrees of freedom.

### C.3.3 Intercept

The intercept is not usually of great interest, but a confidence interval can be obtained for the intercept  $a$  using the formula in the previous section to get a confidence interval for  $y_{fit}$  when  $X = 0$ .



# References

- F.-E. Aballéa. *Propagation acoustique en milieu extérieur: Application de l'équation parabolique rapide au couplage d'effets météorologiques et de topographies complexes*. PhD thesis, Université du Maine, Spécialité Acoustique, France, 2004.
- Swedish Environmental Protection Agency. Ljud från vindkraftverk, report 6241, 2001.
- D.G. Altman. *Practical statistics for medical research*. Chapman&Hall, 1991.
- M. Galindo Arranz. *The parabolic equation method for outdoor sound propagation*. PhD thesis, Technical University of Denmark, Department of Acoustic technology, Denmark, 1996.
- K. Attenborough. Ground parameter information for propagation modeling. *Journal of Acoustical Society of America*, 1992.
- D.J. Auld and K. Srinivas. *Aerospace, mechanical and mechatronic engineering*, 1995.
- P. Botha. The use of 103 wind speed measurements in the assessment of wind farm developments. *Wind turbine noise: Perspective for Control, Berlin*, 2005.
- Brüel and Kjaer. <http://www.bksv.com/pdf/bp0100.pdf>.
- M.E. Delany and E.N. Bazley. Acoustical properties of fibrous absorbent materials. *Appl. Acoust.* 3, 1970.
- O. Fégeant. On the use of a vertical microphone board to improve low signal-to-noise ratios during outdoor measurements. *Applied Acoustics*, 1998.
- J. Forssén. *The influence of atmospheric turbulence on barrier sound reduction*. PhD thesis, Chalmers University of Technology, Department of Applied Acoustics, Sweden, 2001.
- L. Johansson. *Sound propagation around off-shore wind turbines*. PhD thesis, Kungliga Tekniska Högskolan, Department of Civil and Architectural Engineering, Sweden, 2003.
- J. Kragh and B. Sondergaard. Prediction of wind turbine noise propagation over complex terrain in all kinds of weather with nord2000. *Wind turbine noise: Perspective for Control, Berlin*, 2005.
- C. Larsson. Weather effects on outdoor sound propagation. *International Journal of Sound and Vibration*, 2000.

- S. Ljunggren. Iea recommended practices for wind turbine testing and evaluation: 10. measurement of noise immission from wind turbines at noise receptor locations. *1<sup>st</sup> edition*, 1997.
- S. Oerlemans and B. Méndez López. Prediction of wind turbine noise propagation over complex terrain in all kinds of weather with nord2000. *Wind turbine noise: Perspective for Control, Berlin*, 2005.
- M. Ögren. *A study of the measurement of the acoustical ground impedance and its effects*. PhD thesis, Chalmers University of Technology, Department of Applied Acoustics, Sweden, 1999.
- E. M. Salomons. *Computational atmospheric acoustics*. Kluwer Academic Publishers, 2001.
- E. Sloth. Modeling of noise from wind farms and evaluation of the noise annoyance. *Wind turbine noise: Perspective for Control, Berlin*, 2005.
- C. Tickell. Wind turbine noise assessment in australia and comparison of software model predictions for australian conditions and wind farms. *Wind turbine noise: Perspective for Control, Berlin*, 2005.
- G.P. van den Berg. Effects of the wind profile at night on wind turbine sound. *Journal of Sound and Vibration*, 2003.